UNIVERSITY OF CALIFORNIA
RIVERSIDE

Extremely Low-Delay Coding of Gaussian Sources with Side Information at the Decoder

A Dissertation submitted in partial satisfaction
of the requirements for the degree of

Doctor of Philosophy

in

Electrical Engineering

by

Xuechen Chen

March 2012

Dissertation Committee:

Dr. Ertem Tuncel , Chairperson
Dr. Ilya Dumer
Dr. Amit K. Roy-Chowdhury

The Dissertation of Xuechen Chen is approved:

Committee Chairperson

University of California, Riverside

Acknowledgments

I am really grateful to my advisor, Prof. Ertem Tuncel, without whose help, I would not have been here. He has provided me with very valuable ideas, support and encouragement. His enthusiasm on research and perfect personality would make a huge impact on my future career and life. I would never forget all the white-board discussion with him. This dissertation would not have been possible without his guidance.

I would also want to acknowledge the members of my dissertation committee, Prof. Ilya Dumer and Prof. Amit K. Roy-Chowdhury, who have generously given their time and expertise to better my work.

I want to thank my friends and colleagues who gave me help and encouragement during my Phd research and study: Ms. Shuqin Li, Mr. Yang Gao, Dr. Haipeng Ding, Ms. Xuemei Sun, Ms. Puyu Zhang, Dr. Bi Song, Mr. Min Liu, Dr. Yunfan Li, Dr. Yilei Xu, Ms. Miaomiao Luo, Dr. Jing Wu, Mr. Dong Gui, Mr. Shengyang Xu, Ms. Lin Zheng, Mr. Lei Liu. Especially, to Shuqin Li, thank you so much for your encouragement and being a good listener when I felt frustrated; to Xuemei Sun, I really appreciate your self-giving help and kindness.

Finally, I would like to thank to my parents and my dear husband, Sheng Chu, who love me most in the world and give me priceless support. Without them, I couldn't finish my Ph.D. study smoothly.

To Those I Love and Those Who Love Me

ABSTRACT OF THE DISSERTATION

Extremely Low-Delay Coding of Gaussian Sources with Side Information at the Decoder

by

Xuechen Chen

Doctor of Philosophy, Graduate Program in Electrical Engineering
University of California, Riverside, March 2012
Dr. Ertem Tuncel , Chairperson

One of the innovations brought about by the emerging and thriving of wireless sensor networks is Wyner-Ziv (WZ) coding, in other words, lossy source coding with side information at the decoder. While previous work mostly focuses on using capacity-achieving codes to approach the Wyner-Ziv bound, which naturally introduces huge block lengths and huge delay, we study extremely low-delay Wyner-Ziv coding of Gaussian sources. Three related but distinct problems are considered. The first involves scalar quantization and scalar noiseless coding of the quantization indices when only decoder has access to side information. Under high-resolution assumptions and appropriately defined decodability constraints, the optimal quantization level density is conjectured to be periodic. The performance of variable-length coding with uniform quantization is also characterized. The results are then incorporated in predictive Wyner-Ziv coding for Gaussian sources with memory, and optimal prediction filters are numerically designed so as to strike a balance between maximally exploiting both temporal and spatial correlation and limiting the propagation of distortion due to occasional decoding errors. Finally, zero-delay schemes are also employed in transform coding with small block lengths, where the Gaussian source and side information are transformed separately with the premise that

corresponding transform coefficient pairs exhibit good spatial correlation and minimal temporal correlation. For the specific source-side information pairs studied, it is shown that transform coding, even with a small block-length, outperforms predictive coding.

In the second part, we study the zero-delay joint source-channel coding (JSCC) problem of transmitting a Gaussian source over a Gaussian channel in Wyner-Ziv scenario. To achieve zero-delay, after applying scalar quantization to the source, the properly scaled analog information, namely the quantization error, is superimposed on the scaled digital information, i.e., the quantized source, and then transmitted. At the decoder, several decoding schemes are proposed. It is shown that all the schemes, when optimized over all related parameters, are superior to pure analog transmission for high enough correlation between source and side information. The robustness of one of the proposed Hybrid Digital Analog (HDA) schemes against varying channel and side information conditions is also compared with that of the purely analog scheme.

Since JSCC WZ problem is intimately related with JSCC without side information but with bandwidth expansion factor 2, in the third part we investigated the mapping method from 1-D source space to 2-D channel space which integrates HDA schemes into spiral mapping or pure analog mapping. The performance comparison with existing coding algorithms is also presented.

Contents

List of Figures

List of Tables

Chapter 1

Introduction

1.1 Problem Motivation and Background

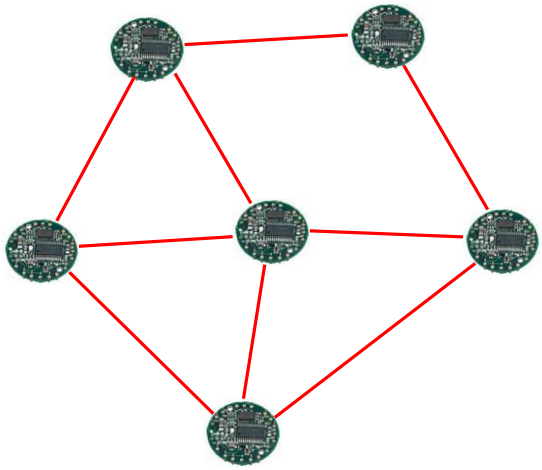

Figure 1.1: The Model of Sensor Network

Sensor research has been emerging and thriving for several decades. Wireless sensor networks that consist of many tiny, low-power, and cheap wireless sensors, shown in Figure 1.1, create a potential that in the near future the physical world will be seamlessly connected to the online world. Unlike PCs or the Internet, which are designed to

support all types of applications, sensor networks are usually mission driven and application specific, which include detection of toxic chemicals; measurement of temperature, pressure, and vibration; or real-time area video surveillance. As a result, wireless sensors must be operated under a set of constraints and requirements. For example, the energy for the network nodes is usually not renewable. This constraint has a crucial impact on the whole operation scheme of wireless sensor networks.

Consider a distributed camera system where cameras image a common scene independently. These sensors transmit their highly correlated information to a central processing unit that forms the best picture of the scene based on the information collected by all of the nodes in the network. It is well-known that standard data compression methods are not the most efficient for this scenario, since they ignore the (high) correlation between the sensor observations. Then, there comes the problem: What could we do to avoid transmission of any "redundant" information when inter-sensor communication is not allowed because of severe power and channel bandwidth constraints? The answer is to use distributed source coding (DSC), where correlated data sequences, observed at different locations in space, are encoded simultaneously and *separately*, to be *jointly* decoded by a central receiver. In contrast with the centralized source coding regimes where multiple sources are available at a single location, e.g., in stereo coding of audio or image signals, the correlation between the observed sequences can only be exploited through the underlying joint statistics, but not through actual realizations of data.

The fundamental question is, how can the sensors exploit the correlation between their measurements without communicating to one another? The answer is best explained using a simple example involving two sensors, where it is given that the measured (integer) temperature values at each sensor, denoted $X(t)$ and $Y(t)$, cannot differ by

more than 1 degree at a given time instant. Let the second sensor transmit its data $Y(t)$ directly, and let the first one transmit $X(t)$ in modulo 3, thereby expending only $\log_2 3$ bits. Using $Y(t)$, $X(t)$ mod 3, and the fact that $|X(t) - Y(t)| \leq 1$, the central unit can uniquely identify $X(t)$. The systematic mapping of the actual data to a limited number of values, as is done by the encoder of $X(t)$ in this example, is usually referred to as *binning* in distributed coding literature. The essence of binning is that the $X(t)$-values placed in the same bin must constitute a "good" channel code for the fictitious channel between $X(t)$ and $Y(t)$, so that given the bin index and the channel output $Y(t)$, the channel codeword $X(t)$ is uniquely identified.

DSC could also be applied to single-camera video coding as was studied in, for example, [1], where motion compensation at the decoder is an effective way to generate reliable side information from previous frames.

If the sensors are measuring 1-D signals, such as temperature, pressure, audio, etc., in addition to low power and bandwidth constraints, another constraint arises: delay. Recent methods that approach theoretical limits of DSC, namely, turbo- or LDPC-like codes require large block lengths to approach the capacity. This, in turn, translates into a large system delay and an increased memory requirement at the sensors even when the employed quantizers are low-dimensional (or scalar). Therefore, it may not be plausible to implement these methods in real-time scenarios, e.g., surveillance for homeland security or monitoring of enemy activity, where low delay is a very crucial requirement.

With these delay-sensitive applications in mind, we develop *extremely low-delay* DSC techniques. In the next few sections, we provide the necessary background before the description of our research in the following chapters.

1.2 Preliminaries and Prior Work

1.2.1 Source Coding

Consider an information source that produces, every unit of time, a symbol x from a finite set $\mathcal{X}$, called the *source alphabet.* Let the source sequence be $X_{n=1}^{\infty}$. Each sample X_n is independent and identically distributed (i.i.d.) with $P_x = \Pr[X = x]$. Then $X_{n=1}^{\infty}$ is called a discrete memoryless source (DMS) if $\mathcal{X}$ is a countable set.

1.2.1.1 Lossless Source Coding

Theorem 1 *AEP(Asymptotic Equipartition Partition): If $X_1, X_2, ...,$ are i.i.d.$\sim p(x)$, then*

$$-\frac{1}{n}\log p(X_1, X_2, ..., X_n) \to H(X) \quad \textit{in probability}$$

This theorem is the analog of the law of large numbers in information theory. Based on AEP, we can define typical set as

Definition 2 *The typical set A_ϵ^n with respect to p(x) is the set of sequences $(x_1, x_2, ..., x_n) \in \mathcal{X}^n$ with the following property:*

$$2^{-n[H(X)+\epsilon]} \leq p(x_1, x_2, ..., x_n) \leq 2^{-n[H(X)-\epsilon]}$$

So all sequences in $\mathcal{X}^n$ could be divided into two sets: the typical set A_ϵ^n and its complement. Typical set has several important properties including:

- For n sufficient large,

$$\Pr[A_\epsilon^n] > 1 - \epsilon.$$

- For any n,

$$|A_\epsilon^n| \leq 2^{n[H(X)+\epsilon]}, \quad \text{where } |A| \text{ denotes the number of elements in the set } A.$$

- For n sufficiently large,

$$|A_\epsilon^n| \geq (1-\epsilon)2^{n[H(X)-\epsilon]}.$$

Based on these properties, we could conclude that lossless representation of sequence X^n can be done with $nH(X)$ bits on the average for sufficiently large n.

Two sequences $(x_1, x_2, ..., x_n)$ and $(y_1, y_2, ..., y_n)$ are jointly typical if the pair is ϵ-typical with respect to the joint distribution p_{XY} and both $(x_1, x_2, ..., x_n)$ and $(y_1, y_2, ..., y_n)$ are ϵ-typical with respect to their marginal distributions p_X and p_Y. The set of all such pairs of sequences is denoted by $A_\epsilon^n(X, Y)$.

1.2.1.2 Lossy Source Coding and Rate Distortion Function

We assume that a transmitted source symbol $X \in \mathcal{X}$ will be reproduced at the destination as a symbol $\hat{X}$ which is an element of another finite set $\hat{\mathcal{X}}$, called the *destination alphabet.* The quality of reproduction is quantified by a distortion measure $d : \mathcal{X} \times \hat{\mathcal{X}} \to [0, \infty)$. And d is usually assumed as a single-letter distortion measure, i.e.,

$$d(\mathbf{X}, \hat{\mathbf{X}}) = \frac{1}{n}\sum_{i=1}^{n} d(X_i, \hat{X}_i).$$

A $(2^{nR}, n)$ rate distortion code consists of an encoding function,

$$f_n : \mathcal{X}^n \to 1, 2, ..., 2^{nR},$$

and a decoding (reproduction) function,

$$g_n : 1, 2, ..., 2^{nR} \to \hat{\mathcal{X}}.$$

The rate R is the number of bits-per-symbol needed to transmit the output of the encoder. A rate-distortion pair (R, D) is called achievable if there exists a sequence of $(2^{nR}, n)$ rate distortion codes (f_n, g_n) with

$$\lim_{n\to\infty} \mathbb{E}d(X^n, g_n(f_n(X^n))) \leq D.$$

The rate distortion region for a source is the closure of the set of achievable rate distortion pairs (R, D). The rate distortion function $R(D)$ is the infimum of rates R such that (R, D) is in the rate distortion region of the source for a give distortion D.

Theorem 3 *The rate distortion function for a DMS is defined as*

$$R(D) = \inf_{P_{\hat{x}|x}:\mathbb{E}d(X,\hat{X})\leq D} I(X;\hat{X}) \tag{1.1}$$

Here the expression $I(X, \hat{X})$ denotes the *mutual information* between random variables X and $\hat{X}$:

$$I(X;\hat{X}) = \sum_{x\in\mathcal{X}}\sum_{\hat{x}\in\hat{\mathcal{X}}} P_x P_{\hat{x}|x} \log \frac{P_{\hat{x}|x}}{P_{\hat{x}}}.$$

$I(X;\hat{X})$ is a convex function of $P_{\hat{x}|x}$. If we focus on finite $\mathcal{X}$ and $\hat{\mathcal{X}}$, the infimum in (1.1) is actually a minimum. And when $D = 0$, from (1.1), $R(0)$ equals to $H(X)$, which coincides with the conclusion of lossless source coding.

1.2.2 Wyner-Ziv Coding

Let $(X_k, Y_k)_{k=1}^{\infty}$ be a sequence of independent drawings of a pair of dependent random variables X, Y, where, $X_k \in \mathcal{X}$, $Y_k \in \mathcal{Y}$. Each pair of sample X_k, Y_k is distributed independently with the same distribution $P_{x,y} = \Pr[X = x, Y = y]$. Then X_k, Y_k are called discrete memoryless sources (DMS) if the source alphabets $\mathcal{X}$ and $\mathcal{Y}$ are both countable sets. Wyner-Ziv coding is concerned with lossy compression of source information X while there is side information Y at the decoder, which is shown in Fig 1.2. But before introducing Wyner-Ziv coding, let us look at the Slepian-Wolf problem [2] for lossless coding first:

Theorem 4 *(Slepian-Wolf): For the distributed source coding problem for the source*

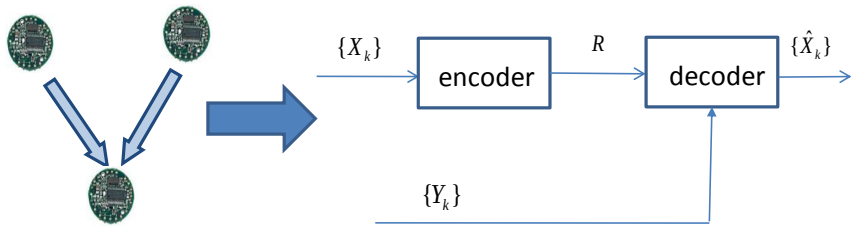

Figure 1.2: The Model of Wyner-Ziv Coding

(X, Y) drawn i.i.d $p(x, y)$, the achievable rate region is given by

$$R_1 \geq H(X|Y)$$

$$R_2 \geq H(Y|X)$$

$$R_1 + R_2 \geq H(X, Y).$$

Next, we introduce the Wyner-Ziv bound.

Theorem 5 *(Wyner-Ziv): The rate distortion function for X with side information Y available only at the decoder is*

$$R_{WZ}(D) = \min_{X,Y,W,f:\mathbb{E}[d(X,f(Y,W)]\leq D} [I(X;W) - I(Y;W)]$$

where W and Y are conditionally independent given X ($Y - X - W$ is a Markov chain).

We provide a sketch of the proof of Theorem 5 for convenience:

- Codebook generation: generate $\mathbf{w}(i) \in \mathcal{W}^n : i = 1, ..., 2^{nR_1}$ randomly and i.i.d. P_W.

- Random binning: for each codeword, generate randomly independently with uniform probability an index $m \in \{1, ..., 2^{nR}\}$. Let $\mathcal{B}$ denote all the codewords associated to index m (we say: in the m-th bin).

- Encoding: given X_n, find $w(i)$ in the codebook such that $(X_n, w(i)) \in A_\epsilon^n(X, W)$. If this is not found, declare error. Then, send index m of the bin containing $w(i)$.

- Decoding: given Y_k and m, find the unique $w(\hat{i}) \in \mathcal{B}(m)$ such that $(Y_n, w(\hat{i})) \in A_\epsilon^n(Y, W)$. If there is no such codeword or more than two codewords found, declare error.

- Error Probability analysis: a codeword $w(i)$ is found with high probability if the codebook is not too small, i.e., if

$$R_1 > I(X, W) + \epsilon$$

  By the Markov lemma, $(Y_n, w(i))$ are jointly typical with high probability, hence, at least one $w(i)$ could be found in bin $\mathcal{B}(m)$. To make it unique, bin should not be too large, i.e.,

$$R_1 - R < I(Y, W) - \epsilon.$$

  It follows that the error probability vanishes as $n \to \infty$ if

$$R > I(X; W) - I(Y; W) + 2\epsilon$$

Figure 1.3 illustrates how binning works. From the figure, we could see that Slepian-Wolf scheme and Wyner-Ziv scheme are intimately related with channel coding. If we treat side information Y as output of "side information channel" while input is source information X, then channel coding principle tells us that with access to Y at the decoder, to reconstruct X, we only need to know the syndrome information of X instead of the whole information. However, in order to achieve the theoretical bound, one has to utilize capacity achieving channel codes (e.g., LDPC, Turbo, etc.), which in turn require very large block lengths. In contrast, our work focuses on low-delay coding

when block length is very small. We still borrow the binning concept in encoder design.

If we denote $R_{X|Y}(D)$ as the rate-distortion function which results when the encoder (as well as the decoder) has access to the side information Y_k, then

$$R_{X|Y}(D) = \min[I(X; \hat{X}|Y)].$$

Slepian-Wolf bound tells us that when $D = 0$, knowledge of the side information at the encoder does not allow a reduction in the transmission rate. In contrast, in nearly all cases it is shown that when $D > 0$ then $R_{WZ}(D) > R_{X|Y}(D)$, which means, knowledge of the side information at the encoder permits transmission of X_k at a given distortion level using a smaller transmission rate. Although $\mathcal{X}$ and $\mathcal{Y}$ are assumed to be finite sets, Theorem 5 is valid in a more general setting which includes the case of Gaussian sources. Interestingly, when X and Y are joint Gaussians, $R_{WZ}(D) = R_{X|Y}(D)$. Specifically, if X and Y are joint Gaussian with zero mean and covariance matrix

$$\begin{bmatrix} 1 & \rho \\ \rho & 1 \end{bmatrix},$$

it turns out that for all $D > 0$

$$\begin{aligned} R_{WZ}(D) &= R_{X|Y}(D) \\ &= \begin{cases} \frac{1}{2}\log\frac{\sigma_X^2(1-\rho^2)}{D} & 0 < D \leq \sigma_X^2(1-\rho^2), \\ 0 & D \geq \sigma_X^2(1-\rho^2). \end{cases} \end{aligned} \tag{1.2}$$

1.2.3 Scalar Quantization

Quantization is the heart of analog-to-digital conversion. We define an $N-$ point scalar (one-dimensional) quantizer Q as a mapping $Q : \mathcal{R} \to \mathcal{C}$ where $\mathcal{R}$ is the real line

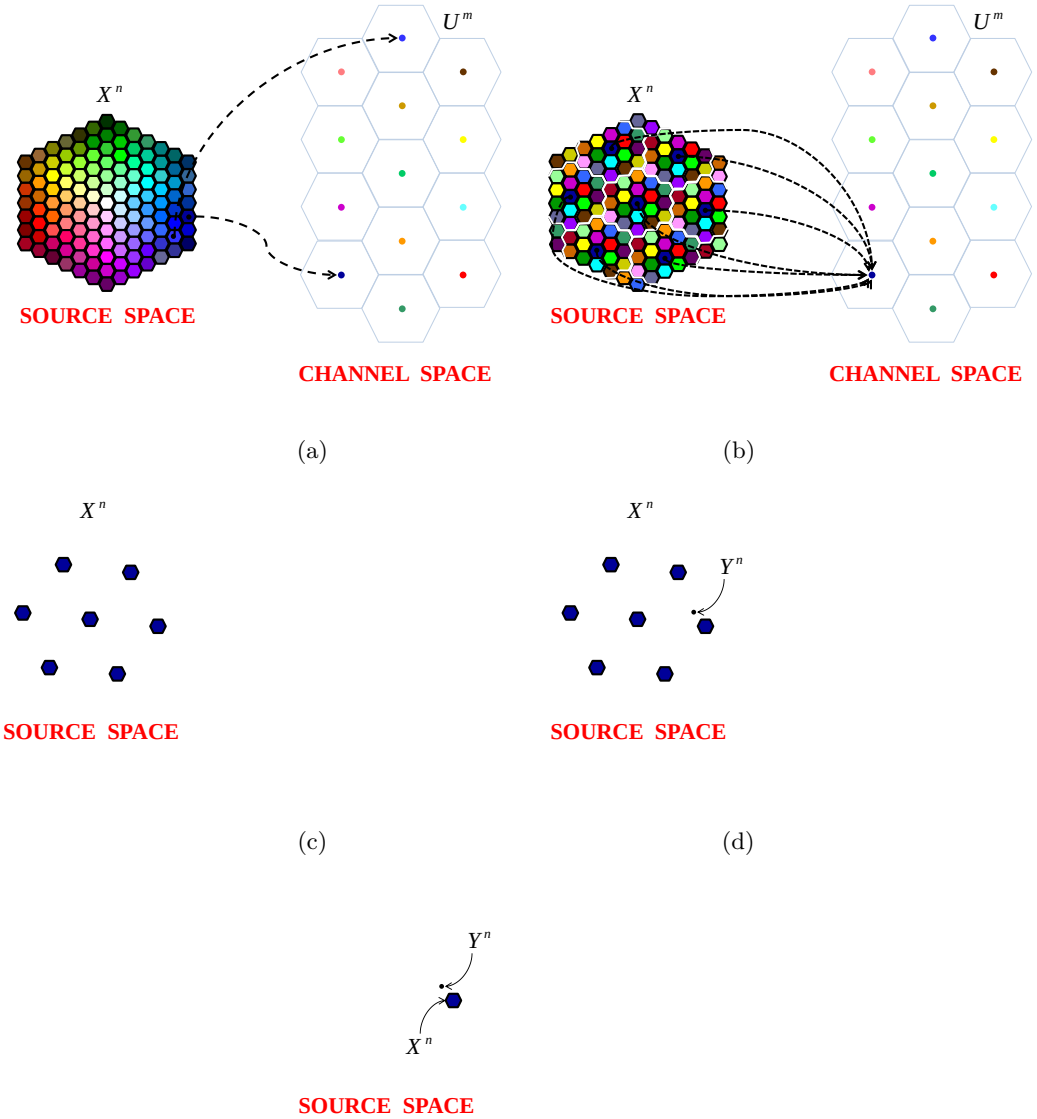

Figure 1.3: . How Binning Works.

and

$$\mathcal{C} = y_1, y_2, y_3, ..., y_N \in \mathcal{R}$$

is the output set or *codebook* with size $|\mathcal{C}| = N$. In all cases of practical interest, N is finite so that a finite number of binary digits is sufficient to specify the output value. We define the resolution or code rate, r, of a scalar quantizer as $r = \log_2 N$ which measures the number of bits needed to uniquely specify the quantized value. The resolution indicates the accuracy with which the original analog amplitude is described. If r is an integer, one can assign to each y_i a unique binary $r-tuple$. In this case a fixed rate code is being used to specify the quantized value. Alternatively, different quantized value can be specified with binary words of differing numbers of digits. In this case, a variable rate code is being used and the *average rate* is the expected number of digits needed to specify the quantized value.

Associated with every N point quantizer is a *partition* of the real line $\mathcal{R}$ into N cells or *atoms* $\mathcal{R}_i$, for $i = 1, 2, ..., N$. The ith cell is given by $\mathcal{R}_i = \{x \in \mathcal{R} : Q(x) = y_i\} = Q^{-1}(y_i)$. A cell that is unbounded is called an *overload* cell. Each bounded cell is called a *granular* cell. Together all of the overload(granular) cells are called the *overload region (granular region).*

A quantizer is defined to be *regular* if

a) each cell R_i is an interval of the form (x_{i-1}, x_i) together with one or both of the end points, and

b) $y_i \in (x_{i-1}, x_i)$.

The values x_i are often called *decision levels.* The values y_i are called *reconstruction levels.* The width of cells or intervals is denoted by Δ_i.

1.2.3.1 Measuring Quantizer Performance

We usually focus most of our attention on the statistical average of the squared error distortion measure and refer to this as the *average distortion.*It is also commonly called the *mean squared error.*

$$D = \mathbb{E}[X - Q(X))^2] = \sum_{i=1}^{N} \int_{R_i} (x - y_i)^2 f_X(x) dx.$$

If the average distortion has value D and the input sequence is stationary and ergodic, then the ergodic theorem implies that with probability one, the limiting time average distortion is also given by D. In this way the more practically meaningful time average of performance can be studied mathematically by the use of statistical averages.

Granular and Overload Noise

The *granular* noise is that component of the quantization error that is due to the granular character of the quantizer for an input that lies within the bounded cells of the quantizer. The *overload* noise is that quantization error that is introduced when the input lies in an overload region of the partition, that is, in any unbounded cell. Generally, granular noise is relatively small in amplitude and occurs to varying degrees with the quantization of each input sample while overload noise can have very large amplitudes but for a well-designed quantizer will occur very rarely. In other words, overload noise depends very strongly on the signal amplitude.

High Resolution Quantization

In most applications of scalar quantization, the number of levels, N, is chosen to be very large so that the quantized output will be a very close approximation to the original input. We shall use the term *high resolution* to refer to the case of quantization when the average distortion is much less than the input variance. Many of the most useful analytical results on quantization require approximate methods of analysis that apply

only to the case of high resolution. High resolution is frequently referred to as "fine quantization" or as "asymptotic" results as they become increasingly accurate as the resolution approaches infinity.

Additive Noise Model of Quantization

Define the quantizer error sequence resulting from applying a quantizer Q to an input signal X_n as $\epsilon_n = X_n - Q(X_n)$. There exists several quantizer noise approximations:

- The signal X_n and the noise ϵ_n are uncorrelated.
- The noise process ϵ_n has a uniform marginal probability distribution.
- The noise process ϵ_n is white, that is, the quantizer noise is an uncorrelated sequence of random variables.

If the input signal is itself stationary and memoryless, then the quantization noise will be white.

Loading Factor

A single parameter that has an important influence on quantizer performance is the *loading factor,* γ, which measures the size of the highest decision level, x_{N-1}, relative to the rms (root mean squared) value σ of the input signal. The loading factor is

$$\gamma = \frac{V}{\sigma}$$

where V is the peak signal magnitude that can be quantized without incurring an excessive overload error.

1.2.3.2 The Uniform Quantizer

A uniform quantizer is a regular quantizer in which (a) the boundary points are equally spaced and (b) the output levels for granular cells are midpoints of the quantization interval. For high resolution uniform quantization, some convenient approximation

can be made to obtain general performance results that are independent of the specific input pdf. Assume the input pdf is sufficiently smooth so that the variation in amplitude of the pdf over any interval of width Δ is very small. Then we can approximate the pdf as having a constant amplitude within a given cell of the partition so that the condition pdf of the error given the input is in the cell of interest is a uniform pdf over the interval $(-\Delta/2, \Delta/2)$. Thus the conditional error has the variance $\Delta^2/12$ and based on the fact that this value is independent of the specific cell, the unconditional mean squared error is approximated by $\Delta^2/12$.

1.2.3.3 The Nonuniform Quantizer

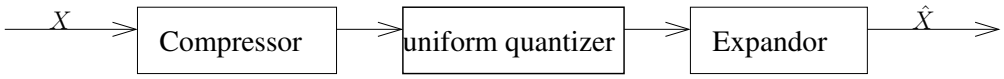

Figure 1.4: The Model of General Nonuniform Quantizer

Nonuniform Quantizer refers to the quantizer that uses nonuniform spacing of quantization levels. A general model for any nonuniform quantizer with a finite number of levels is shown in Figure 1.4. The input x is first compressed by a compressor which has a small slope for large amplitude inputs and therefore compresses of large amplitude values. After going through the uniform quantizer, the expandor reverses the process and expands the large amplitudes. We usually use *compandor* to refer to both the compressor and the expandor. The most important family of compandors is the logarithmic compandors.

1.2.3.4 High Resolution Quantization

We already know that for regular quantizers, an average distortion is given by

$$D = \sum_{i=1}^{N} \int_{x_{i-1}}^{x_i} (x - y_i)^2 f_X(x) dx \tag{1.3}$$

In high resolution case, since N is so large, 1.3 is not convenient for computational use. Based on the idea that for a smooth input pdf and very high resolution quantization, in any local interval of amplitude values, the behavior of the quantizer, is very close to that of a uniform quantizer with a uniform pdf input.

Suppose that with probability nearly one the random variable takes on values in a finite interval (a, b). The quantizer partition divides the finite range (a, b) into N disjoint quantization cells. If the cells are small enough and $f_X(x)$ is smooth enough, the pdf is roughly constant over individual cells, that is, $f_X(x) \approx f_i; x \in \mathcal{R}_i$. Then from the fundamental theorem of calculus, $P_i = \Pr(X \in R_i) = \int_{x_{i-1}}^{x_i} f_X(x) dx \approx (x_i - x_{i-1}) f_i$. Thus we can approximate the average distortion due to granular noise by

$$D = \sum_{i=1}^{N} P_i \int_{x_{i-1}}^{x_i} \frac{(x - y_i)^2}{\Delta_i} dx. \tag{1.4}$$

We know that optimal decoder for a given encoder is $y_i = \mathbb{E}[X|X \in R_i]$. For high resolution case, y_i could be chosen to be the midpoint of the cell. Therefore the integral in 1.4 is just the variance of a uniformly distributed random variable on R_i which is $\Delta_i^2/12$ and hence the approximation becomes

$$D \approx \frac{1}{12} \sum_{i=1}^{N} P_i \Delta_i^2. \tag{1.5}$$

Let $N(x)dx$ denote the number of quantization levels that lie between x and $x + dx$ and assume that as $N \to \infty$ we have a limiting density of reproduction levels

$$\lambda(x) = \lim_{N \to \infty} \frac{N(x)}{N}.$$

which we call the *point density function* for the sequence of quantizers. If there are approximately $N\lambda(x)\Delta_x$ uniformly spaced levels in a cell of length Δ_x, the spacing between the levels must be

$$\begin{aligned}\Delta_i &= \text{width of cell i} \\ &= \frac{\text{length of interval}}{\text{number of levels in the interval}} \\ &= \frac{\Delta_x}{N\lambda(x)\Delta_x} \approx \frac{1}{N\lambda(y_i)}.\end{aligned}$$

So 1.4 can be changed to

$$\begin{aligned}D &\approx \frac{1}{12}\sum_{i=1}^{N} P_i(N\lambda(y_i))^{-2} \\ &\approx \frac{1}{12}\sum_{i=1}^{N} f_X(_i)\Delta_i(N\lambda(y_i))^{-2} \\ &\approx \frac{1}{12}\frac{1}{N^2}\int_{x_1}^{x_{N-1}} f_X(y)\lambda(y)^{-2}dy. \qquad (1.6)\end{aligned}$$

Hölder's inequality states that for any positive a and b with

$$\frac{1}{a}+\frac{1}{b}=1$$

the following inequality holds:

$$\left(\int u(x)v(x)dx\right) \le \left(\int u(x)^a dx\right)^{\frac{1}{a}}\left(\int v(x)^b dx\right)^{\frac{1}{b}}.$$

In the definition for D choose $u(x) = (\frac{f_X(x)}{\lambda^2(x)})^{1/3}, v(x) = \lambda(x)^{2/3}$ and $a = 3$, $b = 3/2$. Then, Hölder's inequality yields

$$\int \frac{f_X(x)}{\lambda^2(x)}^{\frac{1}{3}}[\lambda(x)]^{\frac{2}{3}}dx \le \left[\int \frac{f_X(x)}{\lambda^2(x)}dx\right]^{\frac{1}{3}}\left[\int \lambda(x)dx\right]^{\frac{2}{3}}.$$

Combined with (1.6), we have the bound that

$$D \le \frac{1}{12}\frac{1}{N^2}\left(\int_{V_-}^{V_+} f_X(x)^{1/3}dx\right)^3$$

with equality only if the point density satisfies

$$\lambda(x) = \frac{f_X(x)^{1/3}}{\int f_X(y)^{1/3}dy}.$$

1.2.3.5 Quantization and Variable-Length Scalar Noiseless Coding

A *variable length scalar noiseless code* consists of an encoder f, which maps a single input symbol x into a binary vector $f(x)$ of length $l(x)$, and a decoder g, which maps binary vector $f(x)$ into an output $g(f(x)) = x$. The goal is to keep the average number of bits transmitted for each source symbol as small as possible. For a variable code to be useful, it must be *uniquely decodable* in the sense that if the decoder receives a valid encoded sequence of finite length, there is only one possible input sequence that could have produced the encoded sequence. A more restrictive approach is to require that the code satisfy a prefix condition in the sense that no codeword be a prefix of any other codeword.

The most important fundamental property of a uniquely decodable noiseless source code is given by the *Kraft inequality* described in the following theorem.

Theorem 6 *A necessary and sufficient condition for unique decodability of a noiseless source code with input alphabet* $S = s_0, ..., s_{M-1}$*, encoder* f*, and codeword lengths* $l_k = l(s_k), k = 0, 1, ..., M-1$*, is*

$$\sum_{k=0}^{M-1} 2^{-l_k} \leq 1$$

From the Kraft inequality we have the average length of uniquely decodable code is

$$\begin{aligned} \bar{l}(s) &= \sum_{s \in S} p(s) l(s) \\ &= -\sum_{s \in S} p(s) \log 2^{-l(s)} \\ &\geq -\sum_{s \in S} p(s) \log \frac{2^{-l(s)}}{\sum_{s' \in S} 2^{-l(s')}}. \end{aligned}$$

When the equality holds, $\bar{l}(s) = \sum_{s \in S} p(s) \log \frac{1}{q(s)}$ where $q(s) = \frac{2^{-l(s)}}{\sum_{s' \in S} 2^{-l(s')}}$. Since

$$\begin{aligned} \sum_{s \in S} p(s) \log \frac{1}{p(s)} - \sum_{s \in S} p(s) \log \frac{1}{q(s)} &\leq \log \sum_{s \in S} p(s) \frac{q(s)}{p(s)} \qquad (1.7) \\ &= \log \sum_{s \in S} q(s) \\ &= 0 \end{aligned}$$

where (1.7) follows from Jensen's inequality; $p(s)$ and $q(s)$ are two pmf with a common alphabet S, theorem 7 immediately comes out.

Theorem 7 *Given a uniquely decodable scalar noiseless variable length code, the average length of the code can not be smaller than the entropy of the marginal pmf.*

$$\bar{l}(s) \geq H(p).$$

Moreover, equality holds if and only if $p(s) = 2^{-l(s)}$ *for all* $s \in S$.

Here comes the basic idea of one of the main type of entropy coding. These entropy encoders compress data by replacing each fixed-length input symbol by the corresponding variable-length prefix-free output codeword. The length of each codeword is proportional to the negative logarithm of the probability. Two of the most common entropy encoding techniques are Huffman coding and arithmetic coding.

The output of the quantizer is one of the most common discrete alphabet sources for variable length coding. Assume a regular quantizer Q with quantization cells and reconstruction levels $\mathcal{R}_i, y_i; i = 1, ..., N = 2^R$, where R is the resolution of the quantizer. If the input is a stationary and ergodic process X_n, then the resulting quantized process $Q(X_n)$ is also stationary and ergodic. We should be able to construct a noiseless code for each quantized symbol so that the average bits per sample required is not too much larger than the marginal entropy of the quantized process defined by

$$H_Q = -\sum_{i=1}^{2^R} P(R_i) \log P(R_i).$$

In high resolution regime, $P_i = P(R_i) \approx f_X(y_i)\Delta_i \approx \frac{f_X(y_i)}{N\lambda(y_i)}$. So

$$\begin{aligned} H_Q &= -\sum_{i=1}^{N} \Delta_i f_X(y_i) \log f_X(y_i) - \sum_{i=1}^{N} \Delta_i f_X(y_i) \log \frac{1}{N\lambda(y_i)} \\ &\approx -\int f_X(y) \log f_X(y) dy - \int f_X(y) \log \frac{1}{N\lambda(y)} dy \\ &= h(X) - \mathbb{E}\left[\log \frac{1}{N\lambda(X)}\right] \\ &\geq h(X) - \frac{1}{2}\log 12D, \end{aligned} \tag{1.8}$$

where $h(X)$ is the differential entropy defined by

$$h(X) = -\int f_X(x) \log f_X(x) dx$$

and where (1.8) is due to the fact that

$$D \approx \frac{1}{12}\frac{1}{N^2}\int f_X(y)\lambda(y)^{-2} dy = \frac{1}{12}\mathbb{E}\left(\frac{1}{(N\lambda(X))^2}\right).$$

Equality is achieved in (1.8) if and only if $\lambda(X)$ is a constant, which means quantizer is uniform. Thus we have shown that a uniform quantizer achieves the minimum average distortion

$$D \approx \frac{1}{12} 2^{-2(H_Q - h(X))} \tag{1.9}$$

for a constrained output entropy.

1.2.4 Predictive Quantization

The purpose of data compression is to reduce redundancy. Quantization takes care of the *spatial* redundancy, and prediction attacks *temporal* redundancy.

Closed-Loop Predictive Quantization

The model of closed-loop predictive quantizer is shown in Figure(1.5). The difference e_n between X_n and $\tilde{X}_n$ is quantized, and then the same sequence $\tilde{X}_n$ is added to the quantized value $\hat{e}_n = Q(e_n)$. Here, $\tilde{X}_n$ is actually an estimate of X_n as a "prediction"

from the previously reproduced values according to

$$\tilde{X}_n = -\sum_{i=1}^{m} a_i \hat{X}_{n-i}$$

Simply redraw Figure(1.5), we could find that predictive quantizer has familiar appearance of DPCM (differential pulse code modulation).

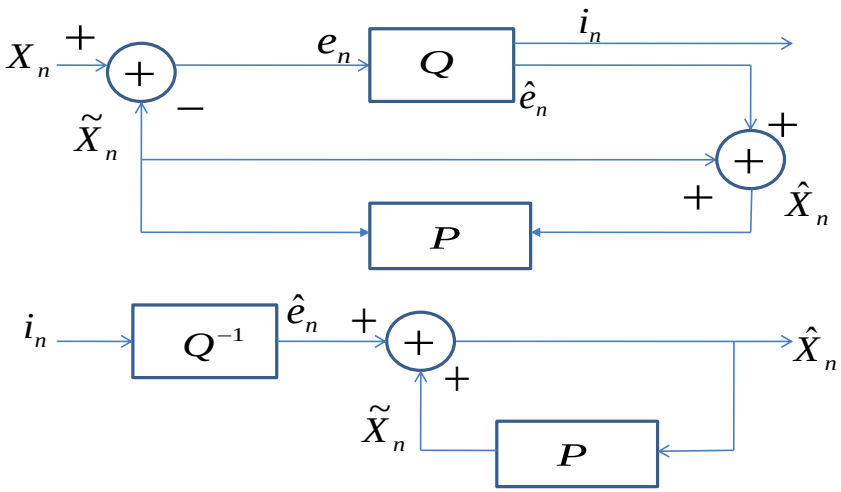

Figure 1.5: The Model of Predictive Quantizer

Theorem 8 ***(Fundamental Theorem of Predictive Quantization)****: The overall mean square reproduction error in predictive encoding is equal to the mean squared error in quantizing the difference signal presented to the quantizer.*

$$\mathbb{E}[(X(n) - \hat{X}(n))^2] = \mathbb{E}[(e(n) - \hat{e}(n))^2]$$

1.2.5 Bit Allocation and Transform Coding

Suppose that we have a block of consecutive samples of a stationary random process. Let X denote the sample vector $X = (X_1, X_2, ..., X_k)^t$. Performing a suitable linear transformation on the input vector X, we can obtain a new vector, Y, also with k components, often called *transform coefficients.* Figure(1.6) illustrates the structure of

transform coding where T is a $k \times k$ invertible matrix that performs the linear transformation. A distinct quantizer is applied to each transform coefficient. A bit allocation strategy is also required for assigning a quota of B bits for the entire vector X under the distortion constraint.

One important case of the linear transformation is orthogonal transformation T which satisfies $T^t = T^{-1}$. The superscript t denotes transpose. The length of a vector is preserved by an orthogonal transformation. This implies that the sum of the squared quantization errors for the k quantizers will be equal to the overall distortion.

$$\mathbb{E}[(X(n) - \hat{X}(n))^2] = \mathbb{E}[(Y(n) - \hat{Y}(n))^2]$$

Karhunen-Loeve Transform

Karhunen-Loeve transform is one kind of orthogonal transform which will make $Y = TX$ have pairwise uncorrelated components. Let $R_x = \mathbb{E}[XX^t]$ denote the autocorrelation matrix of the input vector X. Let u_i denote the eigenvectors of R_X. The Karhunen-Loeve transform matrix is then defined as $T = U^t$, where $U = [u_1 u_2 ... u_k]$.

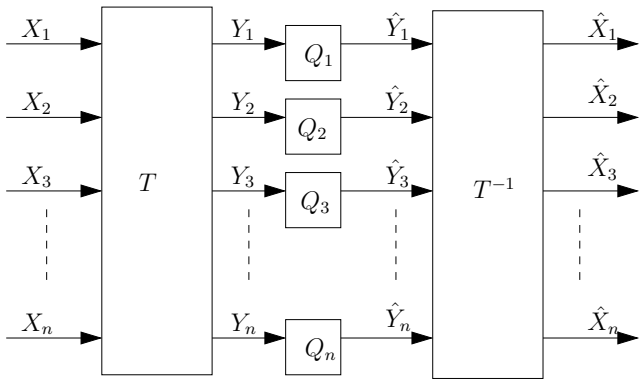

Figure 1.6: The Model of Transform Quantization

1.2.6 Joint Source Channel Coding

Shannon [3] introduced the concept of channel capacity and proved that as long as the transmission rate is below the channel's capacity, reliable communication with a non-zero, but arbitrarily small error rate is possible. He further presented a theorem stating that a source with entropy R can be reliably transmitted over a channel with capacity C as long as $R \leq C$. The theorem could be elaborated after the definitions as below.

Definition 9 *Channel capacity: given the channel's input alphabet A_X and the output alphabet A_Y; for each $\boldsymbol{X} = (x_1, ..., x_n) \in A_X^n$, $b(\boldsymbol{X})$ is the cost of sending $\boldsymbol{x}$. Channel statistics allow us to compute the distribution of the output $\boldsymbol{Y}$. For each positive integer n and $\beta \geq 0$, define $C_n(\beta)$ by*

$$C_n(\beta) = \sup I(\boldsymbol{X;Y}) : \mathbb{E}[b(\boldsymbol{X})] \leq n\beta,$$

then the channel capacity is defined as

$$C(\beta) = \sup \frac{1}{n} C_n(\beta) : n = 1, 2, ...$$

And after elaboration of Theorem 3,

Definition 10 *for each source sequence $\boldsymbol{U} = (u_1, ..., u_k) \in A_U^k$ and corresponding reconstructed sequence $\boldsymbol{V} = (v_1, ..., v_k) \in A_V^k$, the rate distortion function is defined as*

$$R(D) = \inf I(\boldsymbol{U, V}) : \mathbb{E}[d(\boldsymbol{U, V}) \leq D].$$

Define $\bar{\beta} = \frac{1}{n}\mathbb{E}[b(\mathbf{X})]$, $\bar{D} = \frac{1}{k}\mathbb{E}[d(\mathbf{U},\mathbf{V})]$,

Theorem 11 *For a given source and channel, the parameters $\bar{\beta}$, $\bar{D}$ and $\bar{r} = \frac{k}{n}$ must satisfy*

$$\bar{r} \leq \frac{C(\bar{\beta})}{R(\bar{D})}$$

This could be done by firstly applying a source coder to reduce the rate of the source down to the minimum R (remove the redundancy), then applying a channel coder to make the impact of the channel noise on the source as small as possible. In the receiver, the channel decoder, with no idea about the source, outputs the most probable code word to the source decoder. At the final stage, the source decoder reconstructs the source without any knowledge of the channel statistics. This is well known as the *separation* theorem.

There are some shortcomings with the separate coding scheme. First of all, it usually brings in infinite complexity and delay. The hope that it may offer a more favorable performance-delay trade-off is one of the motivations for adopting a joint source-channel coding. Secondly, the "separation principle" is known to fail in certain situations when the source and the channel are nonstationary, as well as in multi-terminal networks. Gastpar et al.[24] gave examples of single-letter codes for single-source systems that perform optimally in the rate-distortion sense. They gave a criterion for determining whether a single-letter code performs optimally for a source-channel pair. We could see the potentiality of omitting channel codes from the article. Thirdly, such systems tend to break down completely when the channel quality falls under a certain threshold, and the channel code is no longer capable of correcting the errors which is known as "threshold effect"; on the other hand, if the channel condition is in fact better, the system can not provide any performance improvement which is known as "leveling-off effect". In other words, the separation system is not strongly robust with respect to changing channel qualities.

Zahir Azami [5] gave a brief overview of the most prominent JSCC techniques known at that time. It covers *unequal error protection, index assignment, multiresolution modulation, co-optimized vector quantizing and direct modulation organising schemes.* Ex-

amples of the latter are *modulation organized vector quantization* which mapped the codewords directly into the modulation plane. In paper [6], the author generalizes several JSCC(Joint Source-Channel Coding) Schemes including digital one, hybrid digital-analogue(HDA) and "Near-Analogue" JSCC Techniques.

For point to point communication with side information at the decoder, the simple analog scale-and-transmit scheme which is well known for its simplicity and optimality when Gaussian source transmitted over an additive white Gaussian noise (AWGN) channel [9], is no longer optimal. Separation principle still works, though, [10]. [7] and [8] both propose one kind of JSCC scheme to achieve optimal mean-squared error (MSE) distortion for the joint Wyner-Ziv and dirty-paper coding. (If the channel interference is set to zero, the problem reduces to Wyner-Ziv coding which we are focusing on.) In the former one, Kochman et al. used high-dimensional modulo-lattice modulation to quantize the source X, and then mapped the analog signal $X - Q(X)$ ($Q(X)$ is the output of quantizer) onto the channel. Wilson et al. [8], proposed with random coding arguments instead of lattice whereby the analog source is integrated into the random codeword.

1.3 Outline of Our Work

In chapter 2, with the motivation of delay-sensitive sensor networks in mind, we study *zero-delay coding* where both the quantization and the noiseless coding of the quantization indices are to be done in a scalar fashion. We employ both non-uniform and uniform quantization followed by fixed- and variable-length coding of indices, respectively. Most existing work on distributed source coding focused on memoryless sources. To exploit the temporal correlation typically found in many sources, we extend

our results to sources with memory by applying prediction filters to both the source and the side information in order to improve efficiency. We then turn to transform coding, where we transform both the source and the side information blocks (of relatively short length) and treat each corresponding transform coefficient pair as a separate *scalar* Wyner-Ziv coding problem. The justification for this approach is that if the source and the side information are highly correlated spatially, then the resultant coefficient pairs will be almost uncorrelated temporally.

In chapter 3, we study the extreme of zero-delay hybrid digital/analog (HDA) schemes for the Wyner-Ziv setup, i.e., the joint source channel coding is to be done in a *scalar* fashion. One of the motivations for applying hybrid digital/analog (HDA) is that we could possibly mitigate the problem bringing by applying pure digital and pure analog systems, which includes that the performance of analog methods would change gradually with channel CSNR and the "threshold", "leveling-off" effects of digital modulation method. HDA transmission could help us achieve not only low delay, but also robustness to channel mismatch when CSI(channel state information) is unknown at the transmitter.

The JSCC WZ problem is intimately related with JSCC without side information but with bandwidth expansion factor 2. In chapter 4, we will discuss the scheme that integrates our zero-delay HDA encoder into channel bandwidth expansion problem especially when expansion factor equals to 2. Some other interesting JSCC mappings for 1 to 2 channel expansion problem include inverse spiral mapping [32],[33] and tent-map mapping [31]. We make a comparison between the performance of our scheme and the one of inverse spiral mapping.

[34] proposed an iterative algorithm to obtain the optimal map between the $k-$dimensional source space and $n-$ dimensional channel space. We have collaborated with them by

rendering our encoder as initial encoder for their iterative algorithm. The detailed description would be described in Chapter 5.

Chapter 2

Low-Delay Prediction- and Transform-Based Wyner-Ziv Coding

This chapter studies low-delay Wyner-Ziv coding, i.e., lossy source coding with side information at the decoder, with emphasis on the extreme of zero-delay coding. To achieve zero-delay, a scalar quantizer is followed by scalar coding of quantization indices. In the fixed-length coding scenario, under high-resolution assumptions and appropriately defined decodability constraints, the optimal quantization level density is conjectured to be periodic. This conjecture, which is provable when the correlation is high, allows for a precise analysis of the rate-distortion tradeoff. The performance of variable-length coding with uniform quantization is also characterized. The results are then incorporated in predictive Wyner-Ziv coding for Gaussian sources with memory, and optimal prediction filters are numerically designed so as to strike a balance between maximally exploiting both temporal and spatial correlation and limiting the propagation of distortion due to occasional decoding errors. Finally, the zero-delay schemes are

also employed in transform coding with small block lengths, where the Gaussian source and side information are transformed separately with the premise that corresponding transform coefficient pairs exhibit good spatial correlation and minimal temporal correlation. For the specific source-side information pairs studied, it is shown that transform coding, even with a small block-length, outperforms predictive coding. Performances of both predictive and transform coding are compared with the asymptotic rate-distortion bounds.

2.1 Introduction

The Wyner-Ziv coding scenario, where a source is to be transmitted in a lossy fashion to a receiver with side information unknown to the sender [4], has received considerable attention over the past decade. Among the most notable contributions is the work of Zamir et al. [11, 12], where the authors proposed a structured algebraic binning scheme based on a pair of nested linear/lattice codes for Wyner-Ziv coding of binary symmetric/quadratic Gaussian sources, where the fine code in the nested pair plays the role of source coding while the coarse code plays that of channel coding. It is shown in [12] that the Wyner-Ziv rate-distortion (RD) function in the quadratic Gaussian case is asymptotically achievable as the dimensionality goes to infinity. Motivated by this, recent research focused on nested lattice codes with fixed-length coding. However, high-dimensional lattice codes are difficult to implement in practice. One approach to mitigate that difficulty is to use trellis-based codes [13]. Another approach is to use low-dimensional lattices (i.e., 1-D or 2-D) followed by ideal Slepian-Wolf coding. Liu et al. [14] proved that, for any finite dimension n and at a fixed high rate R, the performance loss of Wyner-Ziv coding of quadratic Gaussian sources with nested lattice quantization is independent of the source correlation ρ, and observed that the performance loss increases with increasing R for any fixed ρ. They also showed that if ideal Slepian-Wolf coding is assumed for coding of low-dimensional quantization indices,

nested lattice codes come close to Wyner-Ziv RD function for binary symmetric and jointly Gaussian source-side information pairs. Similar approaches were taken in [15, 16, 17]. However, in order to achieve the theoretical Slepian-Wolf rates, one has to utilize capacity achieving channel codes (e.g., LDPC, Turbo, etc.), which in turn require very large block lengths. Though this approach is acceptable for applications such as video coding, it is problematic for sensor network applications, which tend to be delay sensitive.

In this work, with the motivation of delay-sensitive sensor networks in mind, we study *zero-delay coding* where both the quantization and the noiseless coding of the quantization indices are to be done in a scalar fashion. We employ both non-uniform and uniform quantization followed by fixed- and variable-length coding of indices, respectively. In the regime of high resolution, we conjecture that the optimal quantization level density is periodic under the requirement that for every interval of a certain width 2Δ, the number of quantization levels is upper bounded by a given number W. This is a reasonable requirement that makes both the rate and the decoding error probability tractable. We also present the necessary and sufficient condition for the conjecture to hold. Although it proves hard to show the condition is always satisfied, we verify it in two extreme situations: (i) $\rho \to 1$, (ii) $\rho \to 0$. Based on the conjecture, the optimal distributed quantization level density in one period can be computed by solving the usual (non-distributed) quantization level density problem for a new source. The overall RD tradeoff is then obtained by considering all (Δ, W) pairs.

For variable-length coding, we look only at the case where the level density is periodic, as the analysis becomes extremely difficult otherwise. Under the periodicity assumption, the optimal quantizer becomes uniform as in non-distributed variable-length coding.

The periodic characteristic of optimal quantizer was previously postulated in [18], although the authors did not consider the high resolution case. They transformed the original pdf of the source, by periodizing and truncating. They performed Lloyd quanti-

zation on the new pdf and then "periodize" the quantizer without proof of optimality of periodicity. Servetto [19] also explored periodic non-uniform quantization, and claimed that for Gaussian sources, when $\rho \to 1$, the performance loss with respect to Wyner-Ziv RD stays constant as the rate R increases. We compare the performance of our scheme with that in [19], and observe that not only does our scheme outperform Servetto's, but the performance gap between the two schemes widen as $R \to \infty$, and so does that between either scheme and the Wyner-Ziv RD curve (as expected due to [14]). This contrasts with the claim in [19], which is possibly caused by the author's erroneous analysis of non-uniform quantization.

Most existing work on distributed source coding focused on memoryless sources. To exploit the temporal correlation typically found in many sources, we extend our results to sources with memory by applying prediction filters to both the source and the side information in order to improve efficiency. Previously, [20] exploited memory in source coding by applying predictive lattice quantization and Wyner-Ziv DPCM. The author used the prediction filter at the decoder to treat memory as "side information". Generalizing the technique of asymptotic closed-loop predictive quantization to distributed source coding, [21] proposed on iterative algorithm, whereby, binning is included in the loop. In contrast, we place binning after the prediction loop and minimize the combination of the resultant "overload" distortion and the granular distortion obtained prior to binning. After a high-resolution analysis, we arrive at the same conclusion reached immaturely in [22], i.e., that optimal prediction in the Wyner-Ziv regime is fundamentally different from that in non-distributed coding in both fixed-length and variable-length scenarios. The difference stems from two factors: (i) the prediction filters must strike the optimal balance between reducing temporal redundancy and keeping spatial redundancy to maximize coding efficiency, and (ii) at the same time, the prediction filter of the source must suppress the propagation of decoding errors to prevent catastrophic distortion. Our analysis reveals that at low rates, the optimal action is to allow more decoding errors but prevent their propagation aggressively using a very low

prediction coefficient for the source. As the rate increases, it is more advantageous to allow less decoding errors and an increased prediction coefficient. Unfortunately, as was also shown in [23] for zero-delay Wyner-Ziv coding of memoryless sources, our analysis shows that at very high rates, predictive Wyner-Ziv coding has no advantage over its non-distributed counterpart. Fortunately, simulations agree with the high-resolution analysis even at moderate (i.e., practically useful) rates where there is still significant advantage over non-distributed coding. Comparing fixed- and variable-length scenarios, we also observed that (i) in the low rate regime, the performance of the two schemes is almost identical, (ii) at high rates, although the latter shows significant performance gain over the former, both RD curves converge to their non-distributed counterparts, and finally, (iii) the RD performance of variable-length distributed coding is approximately the same as the upper envelope of those of fixed-length distributed and variable-length non-distributed coding schemes.

We then turn to transform coding, where we transform both the source and the side information blocks (of relatively short length) and treat each corresponding transform coefficient pair as a separate *scalar* Wyner-Ziv coding problem. The justification for this approach is that if the source and the side information are highly correlated spatially, then the resultant coefficient pairs will be almost uncorrelated temporally. In fact, if the joint structure of the source $X(n)$ and the side information $Y(n)$ is such that

$$\begin{aligned} X(n) &= T(n) + U(n) \\ Y(n) &= T(n) + V(n) \end{aligned}$$

where $T(n)$ is a stationary Gaussian source and $U(n)$ and $V(n)$ are i.i.d. zero-mean Gaussians independent of each other, then this decorrelation is *exact*. More specifically, if we apply the (ordinary) Karhunen-Loeve transform (KLT) designed for $T(n)$ to both $X(n)$ and $Y(n)$, the corresponding transform coefficient pairs will be *independent*. It should be noted that in this case, although the resultant KLT coincides with the "conditional KLT" for $X(n)$ given $Y(n)$ as introduced by Gastpar et al. [24], the subsequent

bit allocation and coding is different because in [24], transform coefficients from a large number of consecutive blocks are assumed to be jointly encoded in an asymptotically RD-optimal manner. Our approach is also different from that in [25, 26], where the authors studied high-rate scalar quantization of transform coefficients, because ideal Slepian-Wolf coding was assumed for the quantization indices, which still implies very large block lengths.

Our numerical results show that the gap between transform distributed and nondistributed coding is larger than that between predictive distributed and nondistributed coding. Interestingly, when $T(n)$ is a first-order Gauss-Markov process, distributed transform coding even with a small block length performs better than first-order distributed predictive coding. This performance gap is more prominent in fixed-length coding than in variable-length coding. In contrast, for nondistributed coding, the performance of transform coding could catch up with that of predictive coding only after a block length of approximately 50, because first-order prediction of such a source is already very successful in eliminating the temporal redundancy.

Organization of the rest of this paper is as follows. We begin in the next section with optimal fixed-length scalar quantization, and continue with optimal periodic variable-length quantization in Section 2.3. We then incorporate the results in predictive and transform coding in Sections 2.4 and 2.5, respectively. In Appendix A, we briefly discuss the asymptotic Wyner-Ziv rate-distortion function for a certain class of stationary Gaussian sources. Finally, the paper is concluded in Section 2.6.

2.2 High-Resolution Fixed-length WZ Scalar Quantization

We assume that the source-side information pair $(X, Y) \in \mathbb{R} \times \mathbb{R}$ has a probability density function (pdf) that satisfies $p_{XY}(x, y) > 0$ everywhere. Further, the conditional pdf $p_{X|Y}(x|y)$ is a smooth function peaking around $E[X|Y = y]$. A fixed-length code

consists of an encoder-decoder pair

$$\begin{aligned} \phi_{\mathfrak{fl}} &: \mathbb{R} \to \{0,1\}^R \\ \psi_{\mathfrak{fl}} &: \{0,1\}^R \times \mathbb{R} \to \mathbb{R} \end{aligned} \tag{2.1}$$

with $\{0,1\}^R$ denoting all binary strings of length R, where the rate R is assumed to be integer. The resultant average distortion with respect to the squared-error distortion measure $d(x,\hat{x}) = (x-\hat{x})^2$ is given by

$$D = \mathbb{E}[d(X, \psi_{\mathfrak{fl}}(\phi_{\mathfrak{fl}}(X), Y))] \, .$$

2.2.1 Encoder-Decoder Scheme

As shown in Fig. 2.1, we use encoders of the form $\phi_{\mathfrak{fl}} = I_{\text{SW}} \circ Q$, where

1. The quantizer $Q : \mathbb{R} \to \mathbb{Z}$ is a nearest neighbor partition with reconstruction levels $\tilde{x}_j$. We use the notation $\tilde{X} = Q(X)$, and sometimes abuse the notation by using $Q^{-1}(j)$ instead of $\tilde{x}_j$.

2. The Slepian-Wolf (SW) mapping $I_{\text{SW}} : \mathbb{Z} \to \{0, ..., W-1\}$ maps quantizer indices to transmission indices (i.e., "bins"). The corresponding rate becomes $R = \log_2 W$.

We denote by $\hat{X}$ the decoder output, i.e., $\hat{X} = \psi_{\mathfrak{fl}}(\phi_{\mathfrak{fl}}(X), Y)$.

Given the side information $Y = y$ and $i = \phi_{\mathfrak{fl}}(X)$, the optimal decoder would compute

$$\psi_{\mathfrak{fl}}(i, y) = \mathbb{E}[X | Y = y, \phi_{\mathfrak{fl}}(X) = i] \, . \tag{2.2}$$

However, it would be difficult to optimize the end-to-end distortion with respect to the quantizer (and later on, with respect to the prediction filters and transforms) if we use (2.2) and make no further assumptions about the structure of I_{SW}. To that end, we use the simple binning scheme

$$I_{\text{SW}}(j) = j \bmod W$$

and the decoding function

$$\psi(i,y) = \arg \min_{\tilde{x}_j : I_{\mathrm{SW}}(j)=i} |\tilde{x}_j - \mathbb{E}[X|Y=y]| \ . \tag{2.3}$$

Indeed, when the quantizer is of high resolution, it is true that

$$\phi_{\mathrm{fl}}^{-1}(i) \stackrel{\Delta}{=} \{x : I_{\mathrm{SW}}(Q(x)) = i\} \approx \{\tilde{x}_j : I_{\mathrm{SW}}(j) = i\} \ .$$

Therefore, if the reconstruction levels $\tilde{x}_j$ with $I_{\mathrm{SW}}(j) = i$ are sufficiently far apart, (2.3) approximately behaves as the maximum a posteriori estimator for X, thus becoming a competitive alternative to the mean-square estimator (2.2). The special structure of I_{SW} above enforces maximum such separation uniformly for all the bins. Further, to ensure $\hat{X} = \tilde{X}$ with high probability, we enforce that for some large enough $\Delta > 0$, there are at most W reconstruction levels in any interval of length 2Δ on the real axis. Based on (2.3), $\tilde{X} = \tilde{x}_j$ is then correctly decoded when

$$|\tilde{x}_j - \mathbb{E}[X|Y=y]| < \Delta$$

or since $x \approx \tilde{x}_j$, approximately when

$$|X - \mathbb{E}[X|Y=y]| < \Delta \ . \tag{2.4}$$

When (X,Y) is a pair of zero-mean jointly Gaussian random variables whose covariance matrix is

$$\begin{bmatrix} \sigma_X^2 & \rho\sigma_X\sigma_Y \\ \rho\sigma_X\sigma_Y & \sigma_Y^2 \end{bmatrix}$$

the conditional pdf $p_{X|Y}(x|y)$ is also Gaussian with mean

$$\mathbb{E}[X|Y=y] = \frac{\rho\sigma_X}{\sigma_Y} y \tag{2.5}$$

and variance

$$\mathbb{VAR}[X|Y=y] = \sigma_X^2(1-\rho^2) \ . \tag{2.6}$$

It can be seen from (2.4), (2.5), and (2.6) that to achieve a high probability of correct decoding of $\tilde{X}$, one needs to set

$$\Delta = \beta\sigma_X\sqrt{1-\rho^2}$$

with some appropriate large $\beta > 0$, resulting in

$$\Pr[\tilde{X} = \hat{X}] = \mathrm{erf}\left(\frac{\beta}{\sqrt{2}}\right) .$$

We refer to β as the *loading factor* of the quantizer, as it plays the same role as that of a quantizer in non-distributed source coding.

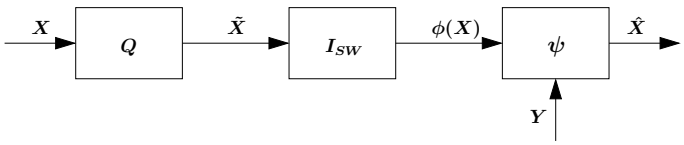

Figure 2.1: The basic encoder-decoder model.

2.2.2 Distortion Analysis

As is well known (see, for example, [29]), the quantizer design problem at high resolution for a given rate R can be formulated in terms of the density of quantization levels $\lambda(x)$. Since the number of levels can be infinite, let this be the "raw" density corresponding to the actual numbers of levels[1]. The density must satisfy

$$\int_{x-\Delta}^{x+\Delta} \lambda(x')dx' \leq W, \quad \forall x \in \mathbb{R} . \tag{2.7}$$

Letting $Z = X - \tilde{X}$, the distortion incurred on X is then given by:

$$\begin{aligned} D &= \mathbb{E}[\big(\hat{X} - X\big)^2] \\ &= \mathbb{E}[\big(\hat{X} - \tilde{X} + \tilde{X} - X\big)^2] \\ &= \mathbb{E}[Z^2] + \mathbb{E}[\big(\hat{X} - \tilde{X}\big)^2] + 2\mathbb{E}[\big(\hat{X} - \tilde{X}\big)Z] \end{aligned}$$

[1]That is, $\lambda(x) = \lim_{N\to\infty} N(x)$ instead of the more commonly used $\lambda(x) = \lim_{N\to\infty} \frac{N(x)}{N}$, where $N(x)dx$ is the number of quantization levels in the interval $(x, x+dx]$.

where

$$D_g = E\big[Z^2\big] \approx \int_{-\infty}^{\infty} \frac{p_X(x)}{12\lambda(x)^2} dx \tag{2.8}$$

is the *granular* distortion correspond to correct decoding of $\tilde{X}$, and

$$D_o = \mathbb{E}[\big(\hat{X} - \tilde{X}\big)^2]$$

is the *overload* distortion resulting from a possible decoding error due to binning. The cross-term $2\mathbb{E}[\big(\hat{X} - \tilde{X}\big)Z]$ is negligible compared to D_o, because

$$\begin{aligned}
\Big|\mathbb{E}[\big(\hat{X} - \tilde{X}\big)Z]\Big| &\leq \mathbb{E}\Big[|\hat{X} - \tilde{X}| \cdot |Z|\Big] \\
&= \mathbb{E}\Big[|\hat{X} - \tilde{X}| \cdot |Z| \Big| \hat{X} - \tilde{X} \neq 0\Big] \Pr[\hat{X} - \tilde{X} \neq 0] \\
&\ll \mathbb{E}\Big[\big(\hat{X} - \tilde{X}\big)^2 \Big| \hat{X} - \tilde{X} \neq 0\Big] \Pr[\hat{X} - \tilde{X} \neq 0] \\
&= \mathbb{E}[\big(\hat{X} - \tilde{X}\big)^2] \,.
\end{aligned}$$

That, in turn, is because for large Δ, the decoding error $\hat{X} - \tilde{X}$ is much larger than the high-resolution quantization error Z in magnitude. Therefore,

$$D \approx D_g + D_o \,. \tag{2.9}$$

2.2.2.1 Analysis of the Granular Distortion D_g

Even in the simplified framework of (2.9), choosing the optimal $\lambda(x)$ minimizing $D_g + D_o$ is a tedious task. Instead, we strive to choose $\lambda(x)$ so as to minimize D_g only. To that end, we start with a conjecture.

Conjecture 12 *The optimal $\lambda^*(x)$ which minimizes (2.8) subject to the constraint (2.7) is periodic with period 2Δ.*

In both [18] and [19], the authors also assumed a periodic quantizer. When $\lambda(x)$ is periodic, we have

$$\begin{aligned} D_g &= \sum_{k\in\mathbb{Z}} \int_{-\Delta+2k\Delta}^{\Delta+2k\Delta} \frac{p_X(x)}{12\lambda(x)^2} dx \\ &= \int_{-\Delta}^{\Delta} \sum_{k\in\mathbb{Z}} \frac{p_X(x'+2k\Delta)}{12\lambda(x'+2k\Delta)^2} dx' \\ &= \int_{-\Delta}^{\Delta} \frac{\sum_{k\in\mathbb{Z}} p_X(x'+2k\Delta)}{12\lambda(x')^2} dx' \end{aligned}$$

using which we can prove the following lemma:

Lemma 13 *The optimal periodic quantizer with period 2Δ is given by*

$$\lambda^*(x) = \frac{W}{C_{X,\Delta}} \left(\sum_{k\in\mathbb{Z}} p_X(x+2k\Delta) \right)^{1/3} \tag{2.10}$$

with

$$C_{X,\Delta} = \int_{-\Delta}^{\Delta} \left(\sum_{k\in\mathbb{Z}} p_X(x+2k\Delta) \right)^{1/3} dx$$

which, using $W = 2^R$, results in

$$D_g(R) = \frac{(C_{X,\Delta})^3}{12} 2^{-2R} \,. \tag{2.11}$$

Proof. Define

$$q_X(x) = \sum_{k\in\mathbb{Z}} p_X(x+2k\Delta)$$

and a corresponding random variable $\check{X}$ such that

$$p_{\check{X}}(x) = \begin{cases} q_X(x) & -\Delta \le x \le \Delta \\ 0 & \text{otherwise.} \end{cases}$$

The granular distortion can then be rewritten as

$$D_g = \int_{-\Delta}^{\Delta} \frac{q_X(x)}{12\lambda(x)^2} dx = \int_{-\Delta}^{\Delta} \frac{p_{\check{X}}(x)}{12\lambda(x)^2} dx$$

It then follows from [29, Section 6.3] and the periodicity of the quantizer that

$$\lambda^*(x) = W \frac{q_X(x)^{1/3}}{\int_{-\Delta}^{\Delta} q_X(x')^{1/3} dx'}$$

where the extra W appears because $\lambda^*(x)$ is the raw density, and must therefore integrate to W over the interval $[-\Delta, \Delta]$. ■

For general (i.e., possibly non-periodic) $\lambda(x)$, one can observe using well-known techniques in calculus of variations that the necessary and sufficient conditions for any $\lambda(x)$ to minimize (2.8) subject to the constraint (2.7) is given by

$$\int_{-\infty}^{\infty} \frac{p_X(x)}{\big(\lambda(x) + \epsilon\mu(x)\big)^2} dx \geq \int_{-\infty}^{\infty} \frac{p_X(x)}{\lambda(x)^2} dx$$

for arbitrary $\epsilon \geq 0$ and $\mu(x)$ satisfying

$$\int_{x-\Delta}^{x+\Delta} \Big(\lambda(x') + \epsilon\mu(x')\Big) dx' \leq W, \quad \forall x \in \mathbb{R} \, .$$

This translates to

$$\frac{d}{d\epsilon} \int_{-\infty}^{\infty} \frac{p_X(x)}{\big(\lambda(x) + \epsilon\mu(x)\big)^2} dx \bigg|_{\epsilon=0} \geq 0$$

or, taking the derivative,

$$\int_{-\infty}^{\infty} \frac{p_X(x)}{\lambda(x)^3} \mu(x) dx \leq 0 \tag{2.12}$$

for any $\mu(x)$ satisfying

$$\int_{x-\Delta}^{x+\Delta} \mu(x') dx' \leq 0, \quad \forall x \in \mathbb{R} \, . \tag{2.13}$$

Now, substituting (2.10) into (2.12), the necessary and sufficient condition for $\lambda^*(x)$ to be the optimal density function becomes

$$\int_{-\infty}^{\infty} \frac{p_X(x)}{q_X(x)} \mu(x) dx \leq 0 \tag{2.14}$$

for any $\mu(x)$ satisfying (2.13). It is easy to observe that if equality in (2.13) holds, which implies $\mu(x)$ is periodic with period 2Δ, then equality in (2.14) would automatically be satisfied.

Although it proved difficult to show (2.14), we could verify it in two extreme situations:

1. When $\Delta \to \infty$, we are effectively performing non-distributed coding. If (2.13) holds, (2.14) would naturally be true, because

$$\lim_{\Delta \to \infty} \frac{p_X(x)}{q_X(x)} = 1$$

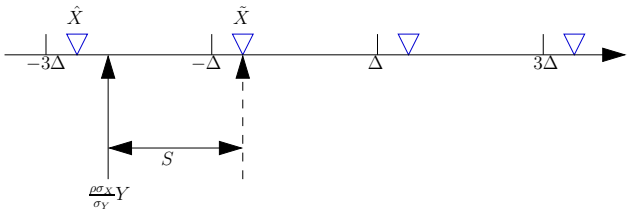

Figure 2.2: A decoding error example. The correct quantized value $\tilde{X}$ is missed because the optimal estimate of X is closer to $\tilde{X} - 2\Delta$. The overload error is $-Q_{2\Delta}(S) = -2\Delta$. The triangles represent all the reconstruction levels $\tilde{X}_j$ with $I_{\mathrm{SW}}(j) = i$, where i is the transmission index

.

uniformly for all x.

2. When $\Delta \to 0$, (2.13) implies that $\mu(x) \leq 0$ for all $x \in \mathbb{R}$. Hence (2.14) is automatically satisfied. The significance of this extreme case is that it corresonds to $\rho \to 1$.

2.2.2.2 Analysis of the Overload Distortion D_o

Defining

$$S = \tilde{X} - \frac{\rho\sigma_X}{\sigma_Y}Y$$

the overload distortion can be written as

$$D_o \approx 4\Delta^2 \sum_{k\in\mathbb{Z},k\neq 0} k^2 \Pr[(2k-1)\Delta \leq S \leq (2k+1)\Delta] \tag{2.15}$$

which follows from $\hat{X} - \tilde{X} = -Q_{2\Delta}(S)$, where $Q_{2\Delta}$ is the uniform quantizer rounding to the nearest integer multiple of 2Δ. This is due to the periodic property of quantizer as we discussed above. See Fig. 2.2 for an illustration.

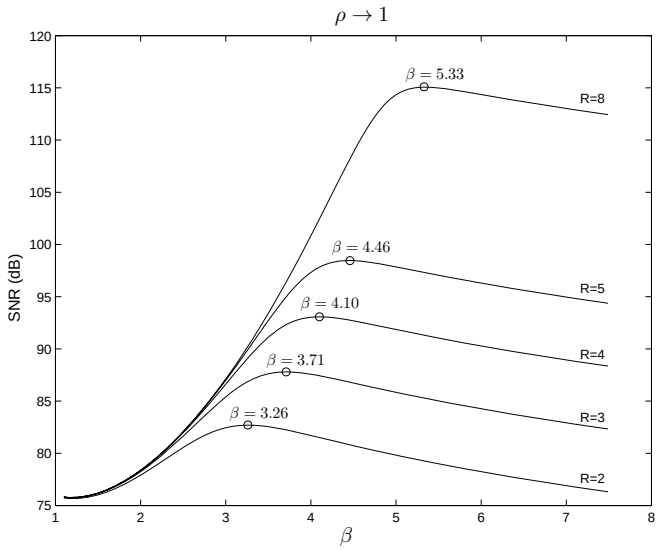

Figure 2.3: Behavior of the total distortion as β varies when $\rho \to 1$. Optimal values of β for various R are also shown.

2.2.2.3 Comparison with Related Work

In [19], Servetto defined a scaling factor s, which plays the same role as Δ here, and argued that for Gaussians it should satisfy:

$$\lim_{\rho \to 1} s(\rho) = 0 \tag{2.16}$$

$$\lim_{\rho \to 1} \frac{s(\rho)}{\sigma_X \sqrt{1-\rho^2}} = \infty \, . \tag{2.17}$$

Our method is different in several aspects. First, we control Δ using β for any ρ, whereas [19] fixes $s(\rho)$. Second, (2.17) implies that $s(\rho)$ shrinks with a rate less than that of $\sigma_{X|Y}$, whereas in our case, the shrinking rate is controlled by the optimum β. Finally, [19] focuses on $\rho \to 1$, while we target all values of ρ. Nevertheless, in the special case of $\rho \to 1$, both granular and overload distortion becomes more tractable analytically in our framework as well. In particular, as $\rho \to 1$, it is clear that $\Delta \to 0$, in which case $p_{\check{X}}(x)$ can be approximated as the uniform distribution. That, in turn, implies that $\lambda^*(x)$ is constant, i.e., the optimal quantizer is uniform, and the corresponding granular distortion can be found as

$$D_g = \frac{\Delta^2}{3} 2^{-2R} \, .$$

Assuming a large enough β, D_o can also be approximated as

$$D_o = E\{(\hat{X} - \tilde{X})^2\} \approx (2\Delta)^2 \left[1 - \text{erf}\left(\frac{\beta}{\sqrt{2}}\right)\right] .$$

Adding the two distortion values together, we obtain

$$D = 4\sigma_X^2(1-\rho^2)\beta^2 \left[\frac{2^{-2R}}{12} + 1 - \text{erf}\left(\frac{\beta}{\sqrt{2}}\right)\right] . \tag{2.18}$$

The behavior of (2.18) as β varies is shown in Fig. 2.3. The optimal β values shown on Fig. 2.3 coincide with what we observed experimentally for very large ρ, thus validating (2.18).

Turning back to general ρ, we see that our $\lambda^*(x)$ differs from the choice of [19], which, although periodic, was given by

$$\lambda(x) = W \frac{p_{X|Y}(x|0)^{1/3}}{\int_{-\Delta}^{\Delta} p_{X|Y}(x'|0)^{1/3} dx'}$$

in the interval $[-\Delta, \Delta]$.

In Fig. 2.4, we compare the performance of our scheme with that in [19]. First of all, as can be seen from the figure, not only is our scheme better, but the performance gap between the two schemes widens as R increases. The second observation is that the gap between the Wyner-Ziv RD curve and the achieved performance of either scheme diverges as $R \to \infty$. Observe that this contrasts with the claim in [19] that the latter gap converges to $G_1 2\pi e$ as $\rho \to 1$, where G_1 is a constant satisfying $\frac{1}{12} \leq G_1 \leq \frac{1}{2}$. We note here that this discrepancy is probably because the expression for distortion derived for uniform quantization in [19, Section III-B] was erroneously applied in [19, Section III-C] for non-uniform quantization.

2.3 High Resolution Variable-Length WZ Scalar Quantization

For variable length coding, on top of the fixed-length encoder $I_{\text{SW}} \circ Q$, with $Q : \mathbb{R} \to \mathbb{Z}$ and $I_{\text{SW}}(j) = j \bmod W$, we also employ a prefix-free mapping $i_{\text{vl}} : [0, 1, ..., W-1] \to$

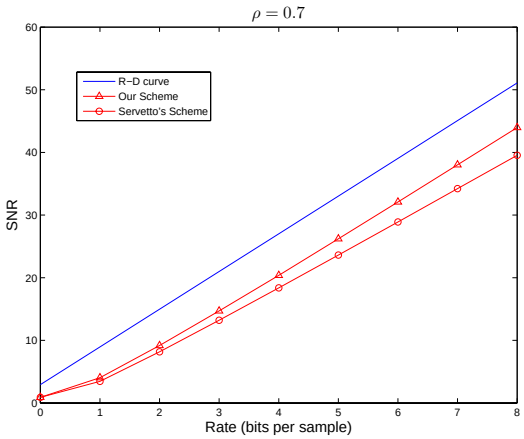

(a)

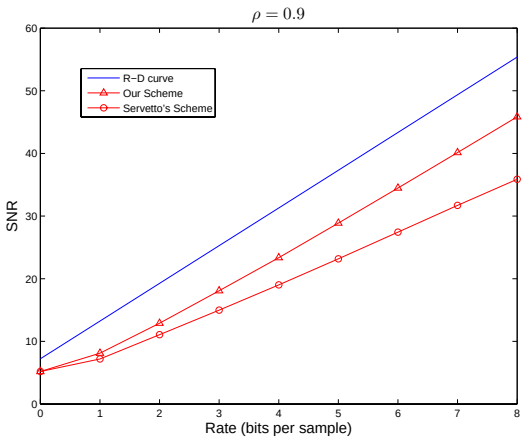

(b)

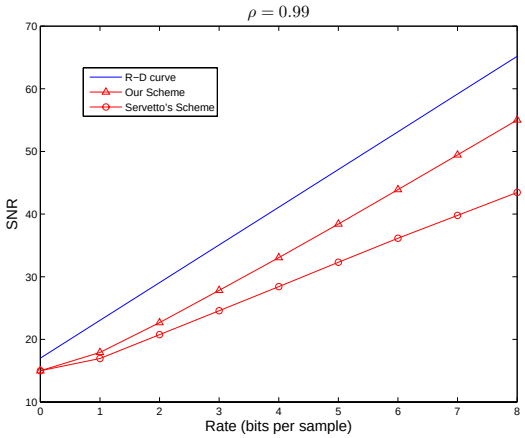

(c)

Figure 2.4: Comparison of the performances of our scheme and Servetto's scheme [19] for different values of ρ.

$\{0,1\}^*$. At the receiver, the variable length codeword is first decoded ignoring the side-information to give the transmission index. The rest of the decoding proceeds as in fixed-length coding.

Since the rate with variable-length coding is a complicated function of the quantizer level density, minimizing the granular distortion for a fixed rate seems to be extremely difficult. Instead, motivated by Conjecture 12, we only look at the case where the level density is periodic. A by-product of this is that the overload distortion is still given by (2.15). The optimal granular distortion is derived in the next lemma.

Lemma 14 *The optimal periodic level density for entropy coded WZ quantization is uniform and the resulting granular distortion is*

$$D_g(R) = \frac{2^{2h(\check{X})}}{12} 2^{-2R} \tag{2.19}$$

where

$$h(\check{X}) = -\int_{-\Delta}^{\Delta} p_{\check{X}}(x) \log p_{\check{X}}(x) dx \ .$$

Proof. The proof follows the same lines as in [29, Section 9.9] after observing that, as in the fixed-length case, designing a periodic WZ quantizer for (X, Y) is no different than designing a non-distributed quantizer for $\check{X}$. This observation leads to

$$D \approx \frac{1}{12W^2} \int_{-\Delta}^{\Delta} \frac{p_{\check{X}}(x)}{\check{\lambda}(x)^2} dx = \frac{1}{12} E\left[\frac{1}{(W\check{\lambda}(\check{X}))^2}\right]$$

and

$$H(\hat{X}) \approx h(\check{X}) - E\left[\log \frac{1}{W\check{\lambda}(X)}\right]$$

where $\check{\lambda}(x) = \frac{\lambda(x)}{W}$. ■

2.4 High-Resolution Predictive WZ coding of Gaussian Sources

2.4.1 Fixed-Length Predictive Coding

Consider two jointly Gaussian processes $X(n)$ and $Y(n)$. We strive for optimal exploitation of time and space correlation by performing scalar Wyner-Ziv coding of $X(n)$ after passing both $X(n)$ and $Y(n)$ through appropriate first-order "prediction" filters $A(z) = 1 - az^{-1}$ and $B(z) = 1 - bz^{-1}$, respectively, as shown in Figure 2.5. The filters need not perform prediction in the classical sense of minimizing the variance of the prediction error. Instead, they need to strike the optimal balance between low time correlation and high space correlation. We denote the filter outputs by $E_X(n)$ and $E_Y(n)$.[2]

The conditional pdf $p_{E_X(n)|E_Y(n)}(e_X|e_Y)$ is Gaussian with mean

$$\mathbb{E}[E_X(n)|E_Y(n) = e_Y] = \frac{\rho_{E_X E_Y}\sigma_{E_X}}{\sigma_{E_Y}} e_Y \tag{2.20}$$

and variance

$$\mathbb{VAR}[E_X(n)|E_Y(n) = e_Y] = \sigma^2_{E_X}\left(1 - \rho^2_{E_X E_Y}\right) \tag{2.21}$$

where

$$\rho_{E_X E_Y} = \frac{R_{E_X E_Y}(0)}{\sigma_{E_X}\sigma_{E_Y}} \ .$$

Similar to S defined in Section 2.2.2.2 to facilitate the analysis of the overload distortion, we could define $S(n)$ as

$$\begin{aligned} S(n) &\stackrel{\Delta}{=} \tilde{E}_X(n) - \frac{\rho_{E_X E_Y}\sigma_{E_X}}{\sigma_{E_Y}} E_Y(n) \\ &\approx E_X(n) - \frac{\rho_{E_X E_Y}\sigma_{E_X}}{\sigma_{E_Y}} E_Y(n) \ . \end{aligned} \tag{2.22}$$

We adopt the same periodic quantization regime as described in the previous section, and optimize over a, b, and β. Unfortunately, unlike in non-distributed predictive source

[2] In the high-resolution quantization regime, the *open-loop* predictor $A(z)$ is a good approximation to the actual *closed-loop* predictor.

coding, we do *not* enjoy the relation

$$\mathbb{E}\left[\Big(X(n)-\hat{X}(n)\Big)^2\right]=\mathbb{E}\left[\Big(E_X(n)-\tilde{E}_X(n)\Big)^2\right]$$

even though we perform closed-loop prediction with matching prediction and reconstruction filters. That is because an encoder-decoder mismatch occurs whenever $|S(n)|>\Delta$. On the other hand, we can redraw the block diagram of our algorithm as in Figure 2.6, from which it can be seen that

$$\begin{aligned}\hat{X}(n) &= \Big[(X(n)+Z(n))\star a(n)-\hat{S}(n)\Big]\star a^{-1}(n)\\ &= X(n)+Z(n)-\hat{\hat{S}}(n) \qquad (2.23)\end{aligned}$$

where $\star$ denotes convolution, $a(n)$ and $a^{-1}(n)$ are respectively the impulse responses of the prediction filter $A(z)=1-az^{-1}$ and the reconstruction filter $A^{-1}(z)=\frac{1}{1-az^{-1}}$, and

$$\hat{\hat{S}}(n)=\hat{S}(n)\star a^{-1}(n)\ . \qquad (2.24)$$

But, (2.23) together with the high resolution assumption implies

$$\begin{aligned}D &= \mathbb{E}\left[\Big(\hat{X}(n)-X(n)\Big)^2\right]\\ &\approx \mathbb{E}\left[Z(n)^2\right]+\mathbb{E}\left[\hat{\hat{S}}(n)^2\right]\\ &= D_g+D_o\ .\end{aligned}$$

where, the cross-term $\mathbb{E}[Z(n)\hat{\hat{S}}(n)]$ vanishes as before.

It is a tedious task to choose the optimal $\lambda(e_X)$ minimizing D_g+D_o. Instead, we choose $\lambda(e_X)$ so as to minimize D_g only, and as discussed above, it becomes

$$\lambda(e_X)=\frac{W}{C_{E_X,\Delta}}\Big(\sum_{k\in\mathbb{Z}}p_{E_X(n)}(e_X+2k\Delta)\Big)^{1/3} \qquad (2.25)$$

for any $e_X\in\mathbb{R}$, where

$$C_{E_X,\Delta}\triangleq\int_{-\Delta}^{\Delta}\Big(\sum_{k\in\mathbb{Z}}p_{E_X(n)}(e_X+2k\Delta)\Big)^{1/3}de_X\ .$$

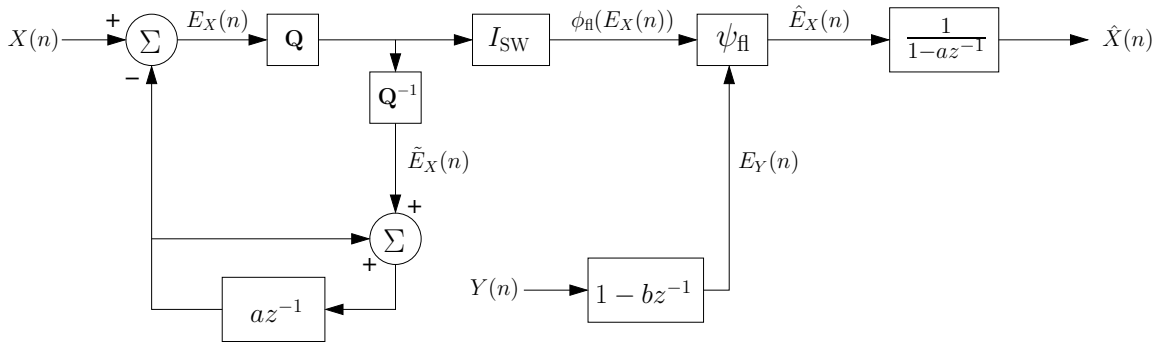

Figure 2.5: Predictive Wyner-Ziv coding.

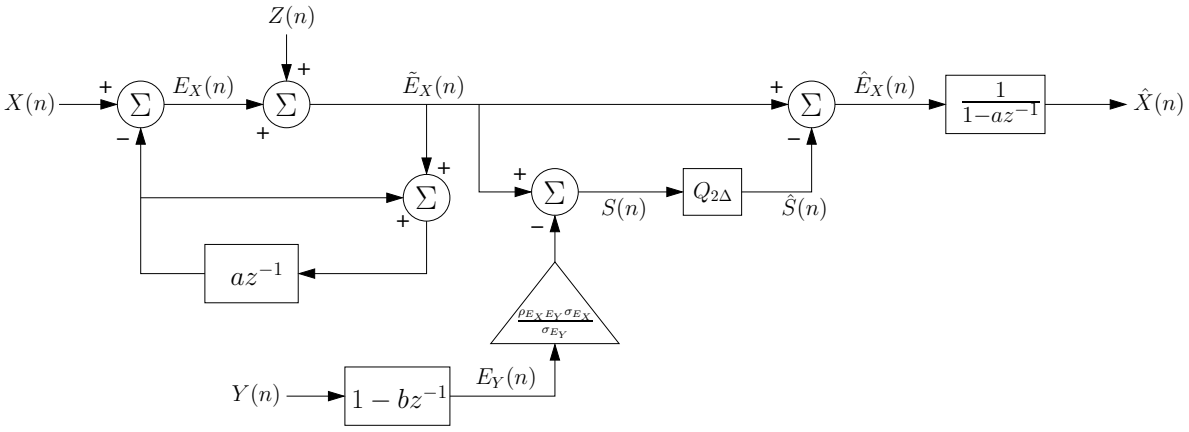

Figure 2.6: An equivalent block diagram in the high-resolution regime.

The corresponding minimum granular distortion is then given by

$$D_g \approx \frac{(C_{E_X,\Delta})^3}{12} 2^{-2R} \tag{2.26}$$

We have from (2.24) that

$$\mathbb{E}\left[\hat{\hat{S}}(n)^2\right] = R_{\hat{\hat{S}}\hat{\hat{S}}}(0) = \sum_{\tau=-\infty}^{\infty} \frac{|a|^\tau R_{\hat{S}\hat{S}}(\tau)}{1-a^2} \tag{2.27}$$

where

$$R_{\hat{S}\hat{S}}(\tau) = 4\Delta^2 \sum_{i=-\infty}^{\infty} \sum_{j=-\infty}^{\infty} ij \Pr[\hat{S}(n) = 2i\Delta, \hat{S}(n-\tau) = 2j\Delta]$$

which reduces to the *unfiltered* overload distortion in (2.15) when $\tau = 0$, as it should. To evaluate

$$\begin{aligned} &\Pr[\hat{S}(n) = 2i\Delta, \hat{S}(n-\tau) = 2j\Delta] \\ &= \int_{(2i-1)\Delta}^{(2i+1)\Delta} \int_{(2j-1)\Delta}^{(2j+1)\Delta} p_{S(n)S(n-\tau)}(s_1, s_2) ds_1 ds_2 \end{aligned}$$

we use the approximation (2.22) which makes $S(n)$ a Gaussian process with zero-mean and autocorrelation

$$\begin{aligned} R_{SS}(\tau) &= R_{E_X E_X}(\tau) + \frac{\rho^2_{E_X E_Y} \sigma^2_{E_X}}{\sigma^2_{E_Y}} R_{E_Y E_Y}(\tau) \\ &\quad - \frac{\rho_{E_X E_Y} \sigma_{E_X}}{\sigma_{E_Y}} \left[R_{E_X E_Y}(\tau) + R_{E_X E_Y}(-\tau) \right]. \end{aligned}$$

It can be deduced from (2.27) that if $|a| \approx 1$, (i) even occasional decoding errors will propagate for a long time, and (ii) these errors will be amplified immensely by a factor $\frac{1}{1-a^2}$. Conversely, if $a \approx 0$, then $R_{\hat{\hat{S}}\hat{\hat{S}}}(0) \approx R_{\hat{S}\hat{S}}(0)$, and overload distortion will be given by (2.15), i.e., binning errors will be forgotten quickly and will not be amplified.

The choice of a, b, and β affect both D_g and $R_{\hat{S}\hat{S}}(\tau)$ in so complex a manner that analytical optimization is an almost hopeless task. We instead use experimental analysis and perform a brute-force search in the space $-1 < a, b < 1$ and $\beta \geq 2.5$. In our experiment, we use the following model. Let $T(n)$ be a first-order Gauss-Markov process. That is,

$$T(n) = \rho T(n-1) + W(n)$$

where $W(n)$ is i.i.d. zero-mean Gaussian, $W(n) \perp T(n-1)$, and $\sigma_W^2 = 1 - \rho^2$ so that $\sigma_T^2 = 1$. Also assume that $T(0)$ has zero mean and unit variance so that the process is stationary. Let the source $X(n)$ observed at the encoder and the side information $Y(n)$ observed at the decoder be noisy observations of $T(n)$, i.e.,

$$X(n) = T(n) + U(n) \tag{2.28}$$

$$Y(n) = T(n) + V(n) \tag{2.29}$$

where $U(n)$ and $V(n)$ are i.i.d. zero-mean Gaussians independent of each other.

Figures 2.7(a), (b), and (c) show the resultant high-resolution rate-distortion performance for three sample cases in which the space correlation is high enough. Also shown on the same figures are the high-resolution rate-distortion performances when (i) the *naive* choice of filter parameters $a = \frac{\rho}{1+\sigma_U^2}$ and $b = \frac{\rho}{1+\sigma_V^2}$ is used[3], and (ii) the side information at the decoder is ignored. Optimal β increases without bound as we climb up the rate-distortion curve. Thus, as $R \to \infty$, the scalar Wyner-Ziv coder reduces to a scalar non-distributed coder, explaining why all three curves meet at high rates, and also why the optimal choice of a approaches the naive one. Since the high-resolution assumption is accurate only at high rates, one may wonders whether any of our analysis is useful. To address this, we implemented actual quantizers corresponding to $\lambda(e_X)$ and simulated the coding of sequences of length 1,000,000. Fortunately, as shown also on Figures 2.7(a), (b), and (c), the simulated performance is not only always better than that of non-distributed source coding, but also catches the theoretical performance at moderate rates where there is still room for Wyner-Ziv coding gain.

On the low rate side, since optimal β is also low, the decoding error probability becomes high, resulting in the need to quickly forget the errors as discussed above. This explains the very low values a assumes at low rates.

Finally, Figures 2.7(a), (b), and (c) also show the corresponding asymptotically optimal rate-distortion performances, i.e., when arbitrarily large *block*-codes are allowed. We

[3]This choice minimizes $\sigma_{E_X}^2$ and $\sigma_{E_Y}^2$ simultaneously, and corresponds to the optimal first-order prediction filters in non-distributed source coding.

defer the detailed computation of the asymptotic rate-distortion curve to Appendix A.

2.4.2 Variable-Length Predictive Coding

We use the same coding technique as in Figure 2.6. Therefore, the overload distortion D_o is the same as in fixed-length predictive coding. However, the granular distortion $\mathbb{E}[Z^2(n)]$ has to be reformulated. Following (2.19),

$$D_g = \mathbb{E}[Z^2(n)] = \frac{2^{2h(\check{E}_X)}}{12} 2^{-2R}$$

where

$$h(\check{E}_X) = -\int_{-\Delta}^{\Delta} p_{\check{E}_X}(e_X) \log p_{\check{E}_X}(e_X) de_X \tag{2.30}$$

and

$$p_{\check{E}_X}(e_X) = \begin{cases} \sum_{k\in\mathbb{Z}} p_{E_X}(e_X + 2k\Delta) & -\Delta \le e_X \le \Delta \\ 0 & \text{otherwise} \end{cases}.$$

Figures 2.8(a), (b), and (c) show the resultant high-resolution rate-distortion performance for the same sample cases as in fixed-length predictive coding. The behavior of optimal a and β is similar to what we observed in fixed-length coding. Also similar are (i) how the gap between optimal distributed and non-distributed coding performances vanish as the rate increases, and (ii) how the simulated performance is superior to non-distribued coding even in low rates.

We also compare the performance of fixed- and variable-length scenarios in Figure 2.9 for the same three cases. In the low rate regime, the performance of fixed- and variable-length distributed schemes is almost identical. This is expected, as in the low rates, β (and thus Δ) tends to be low, which results in an almost uniform $p_{\check{E}_X}$. On the other hand, at high rates, although there is a significant gap between the two, both converge to their non-distributed counterparts as β becomes very large. It is interesting to observe that even at medium rates, where there is *potential* for variable-length distributed coding to have a significant gain over *both* fixed-length distributed coding and

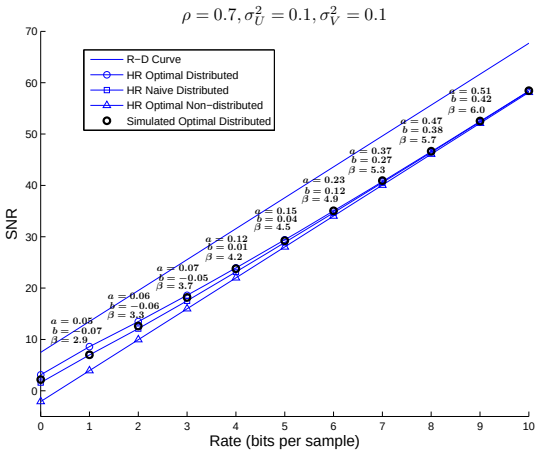

(a)

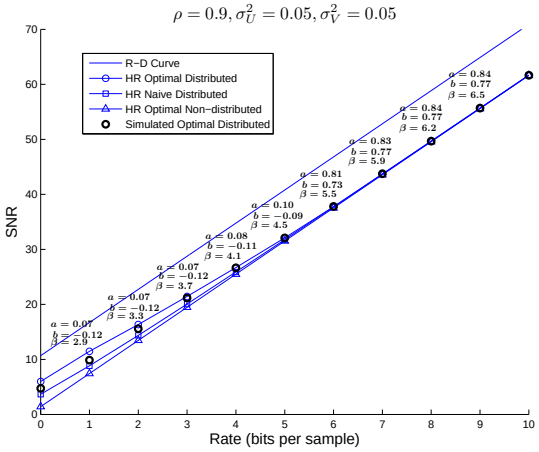

(b)

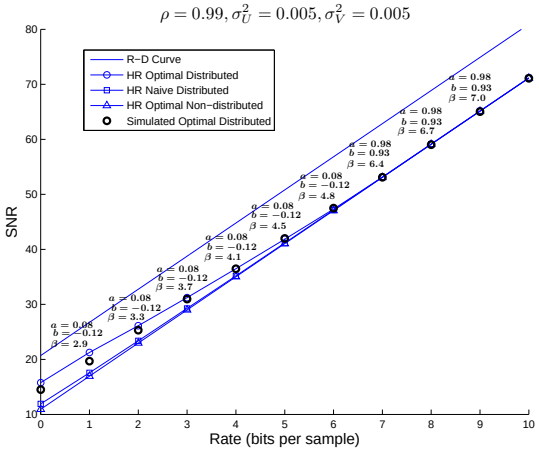

(c)

Figure 2.7: Comparison of the rate-distortion performance of various schemes for three sample source parameters using fixed-length predictive coding. Optimal a, b, and β are indicated on the curves.

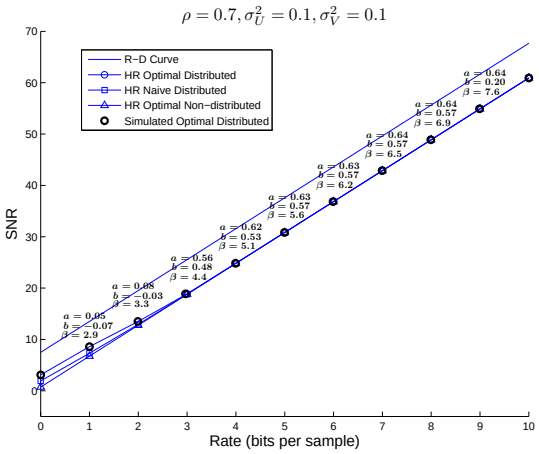

(a)

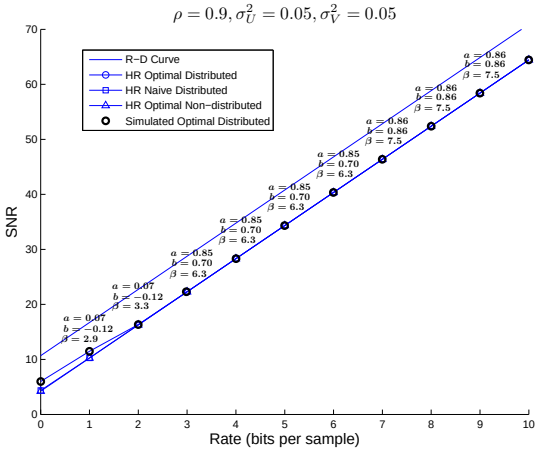

(b)

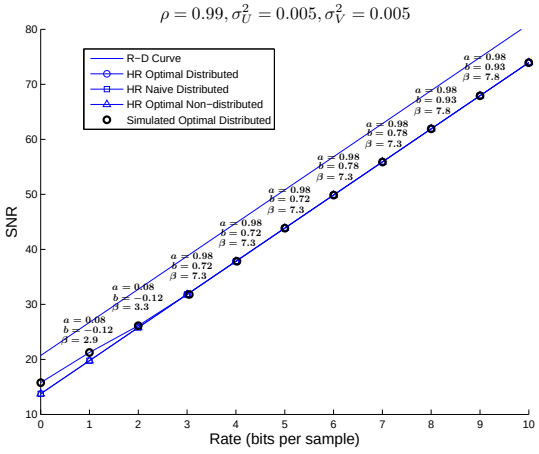

(c)

Figure 2.8: Comparison of the rate-distortion performance of various schemes for three sample source parameters using variable-length predictive coding. Optimal a, b, and β are indicated on the curves.

variable-length non-distributed coding, that potential is not realized. In other words, the rate-distortion performance of variable-length distributed coding is approximately the same as the upper envelope of those of fixed-length distributed and variable-length non-distributed coding schemes.

2.5 High Resolution Transform WZ Coding of Gaussian Sources

Our transform coding model is as shown in Figure 2.10. In this section, we exploit the structure of $X(n)$ and $Y(n)$ as given in (2.28) and (2.29) with arbitrary stationary Gaussian $T(n)$ to design optimal transform matrices $\mathbf{A}$ and $\mathbf{B}$. More specifically, the $k \times k$ covariance matrices $\mathbf{C}_{XX}$, $\mathbf{C}_{YY}$, and $\mathbf{C}_{XY}$ can be written as

$$\begin{aligned} \mathbf{C}_{XX} &= \mathbf{C}_{TT} + \sigma_U^2 \mathbf{I} \\ \mathbf{C}_{YY} &= \mathbf{C}_{TT} + \sigma_V^2 \mathbf{I} \\ \mathbf{C}_{XY} &= \mathbf{C}_{TT}. \end{aligned}$$

In the transform domain, the corresponding covariance matrices become

$$\begin{aligned} \mathbf{C}_{X'X'} &= \mathbf{A}\mathbf{C}_{TT}\mathbf{A}^{-1} + \sigma_U^2 \mathbf{I} \\ \mathbf{C}_{Y'Y'} &= \mathbf{B}\mathbf{C}_{TT}\mathbf{B}^{-1} + \sigma_V^2 \mathbf{I} \\ \mathbf{C}_{X'Y'} &= \mathbf{A}\mathbf{C}_{TT}\mathbf{B}^{-1}. \end{aligned}$$

Thus, setting both $\mathbf{A}$ and $\mathbf{B}$ to the Karhunen-Loeve transform (KLT) for the vector source $T(1), T(2), \ldots, T(k)$, one can make all three matrices diagonal. This, in turn, implies that the transform coefficient pairs $(X_1', Y_1'), (X_2', Y_2'), ..., (X_k', Y_k')$ are independent of each other, and therefore, should be coded separately after proper allocation of the available bits.

It should be noted that in this case, although our transform coincides with the "conditional KLT" for $X(n)$ given $Y(n)$ as introduced by Gastpar et al. [24], the subsequent

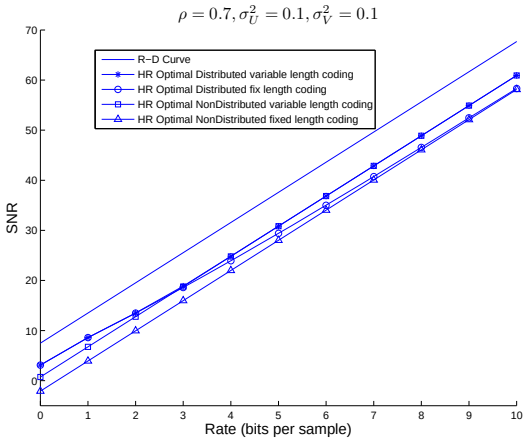

(a)

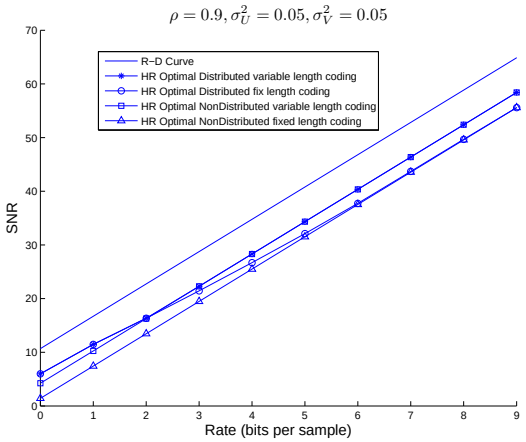

(b)

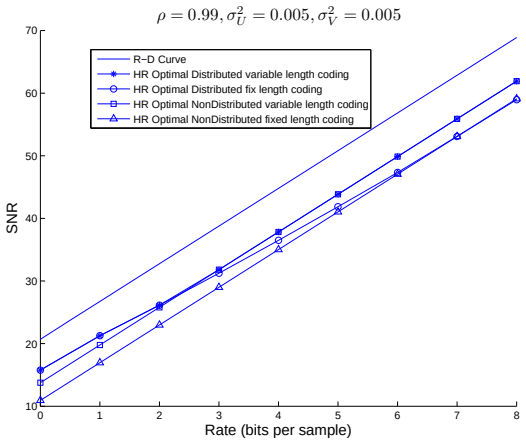

(c)

Figure 2.9: Comparison of the rate-distortion performance of fixed length and variable length predictive coding

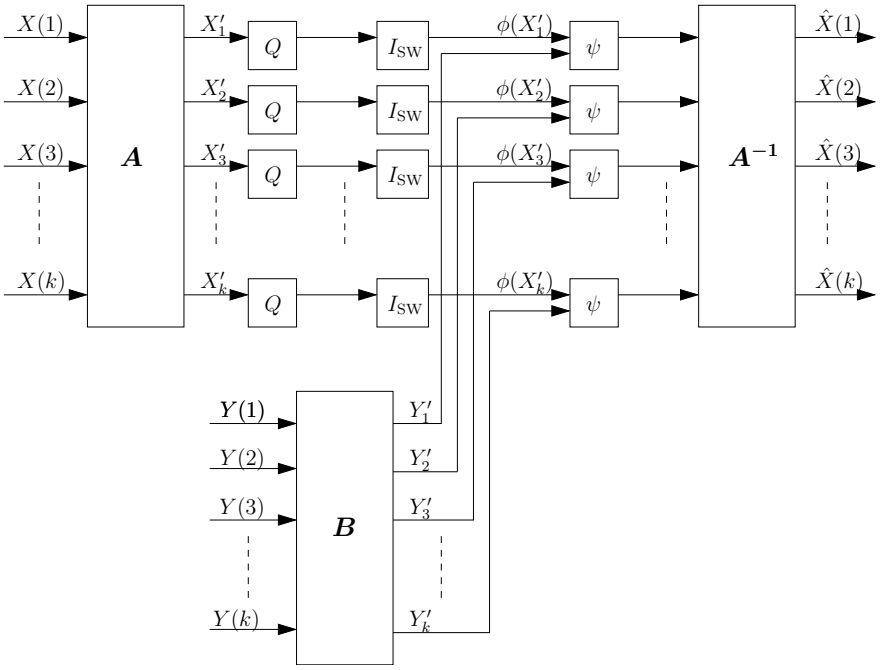

Figure 2.10: Transform Wyner-Ziv coding by scalar coding of corresponding transform coefficients.

bit allocation and coding is different because in [24], transform coefficients from a large number of consecutive blocks are assumed to be jointly encoded in an asymptotically RD-optimal manner.

The average distortion on $X(1), \ldots, X(k)$, or equivalently on $X'_1, \ldots, X'_k$, can be written as

$$D(b_1, b_2, \ldots, b_k) = \frac{1}{k} \sum_{i=1}^{k} D_i(b_i)$$

where $b_1, \ldots, b_k$ are the number of bits allocated to component i so that

$$\sum_{i=1}^{k} b_i = kR$$

and $D_i(b_i)$ is the distortion of the ith transform coefficient, which, as before, comprises of granular and overload components:

$$D_i(b_i) = D_{g,i}(b_i) + D_{o,i} \ .$$

Depending on whether fixed- or variable-length coding is used, $D_{g,i}(b_i)$ can be calculated as in (2.11) or (2.19), respectively, using X'_i in place of X. Similarly, $D_{o,i}$ is given as in

(2.15) using

$$S_i' = X_i' - \frac{\rho_{X_i'Y_i'}\sigma_{X_i'}}{\sigma_{Y_i'}} Y_i'$$

in place of S. Of course, for each integer b_i, the parameter Δ should be chosen so as to minimize $D_i(b_i)$.

We convexify $D_i(b_i)$ so that $D(b_1, b_2, \ldots, b_k)$ becomes convex as well, in which case the bit allocation problem

$$\begin{aligned} \text{Minimize} \quad & \sum_{i=1}^{k} D_i(b_i) \\ \text{subject to} \quad & \sum_{i=1}^{k} b_i = kR \end{aligned} \tag{2.31}$$

can alternatively be tackled by minimizing the Lagrangian

$$L = \sum_{i=1}^{k} \Big[D_i(b_i) + \lambda b_i \Big] \triangleq \sum_{i=1}^{k} L_i$$

for every $\lambda > 0$. It is clear that the minimum is achieved by independently minimizing each L_i. That, in turn, implies that as we initialize λ as a sufficiently large number and gradually decrease it, we can successfully track the optimal $\{b_i\}_{i=1}^k$ by the following simple algorithm.

1. Initialize with $b_i = 0$ for all i.
2. Calculate $\delta_i = D_i(b_i) - D_i(b_i + 1)$.
3. Find $i^* = \arg\max_i \delta_i$, and increment b_{i^*}.
4. Repeat 2 and 3 until $\sum_i b_i = kR$.

This algorithm is essentially the same as that given in [29, Section 16.5], where the lower envelope of $\sum_{i=1}^{k} [D_i(b_i) + \lambda b_i]$ for all possible bit assignments was treated as a piecewise linear monotonically increasing function of λ, and *singular* values of λ where two line segments meet are visited until the desired number of total bits is reached. In our algorithm, each maximum δ_i corresponds to the next singular λ to be visited.

For the same Gauss-Markov $T(n)$ as in predictive coding, with $\rho = 0.99$ and $\sigma_U^2 = \sigma_V^2 = 0.005$, we compare the performance of distributed transform coding to those of predictive coding as well as non-distributed coding in Figure 2.11. Figures 2.11(a) and (b) show how the performance of transform coding (both distributed and non-distributed) evolves with increasing block-length for fixed- and variable-length coding, respectively. Figures 2.11(c) and (d) compare the performance of transform coding to that of predictive coding, again for fixed- and variable-length coding, respectively. Finally, Figure 2.11(e) compares the performance of fixed- and variable-length predictive and transform coding.

First of all, we observe that the gap between distributed and non-distributed transform coding is larger than that between distributed and non-distributed predictive coding. Secondly, distributed transform coding yields better results than distributed predictive coding, contrary to the non-distributed case. This can be explained by the fact that the source $X(n)$ is *nearly* first-order Markov, and first-order prediction is thus very powerful in non-distributed coding. In fact, we had to increase the block-length to 50 for transform coding to catch up with predictive coding. On the other hand, due to the fact that significant temporal correlation remains after prediction in the distributed case, the performance of predictive coding falls below that of transform coding.

2.6 Conclusion

We studied zero-delay, i.e., scalar, lossy source coding with side information at the decoder. Instead of imposing a periodic structure on the scalar quantizer directly, we addressed optimal quantization under the constraint that within every interval of size 2Δ, there are at most W cells. We conjectured that optimal quantizers under this regime are periodic, and proved this conjecture for the important extreme case of a very high correlation coefficient between the source and side information.

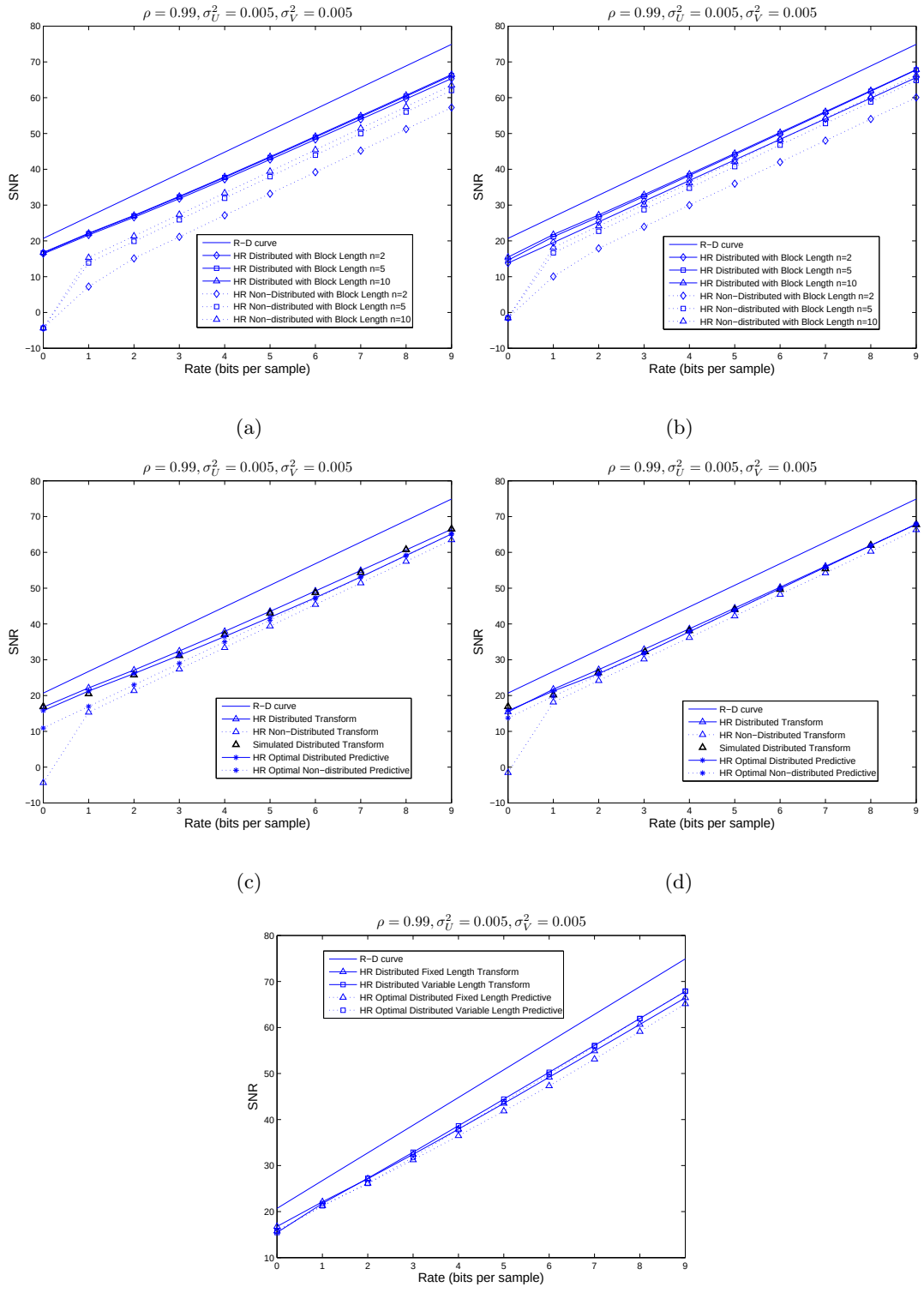

Figure 2.11: Transform coding results. (a) and (b) compare the performances with various block-lengths for fixed- and variable-length coding, respectively. (c) and (d) compare the performance of transform coding (with block-length 10) and predictive coding (with order 1) for fixed- and variable-length coding, respectively. Finally, (e) compares fixed- and variable-length coding for both transform and predictive coding.

When we incorporated our zero-delay coding results into predictive coding for Gaussian sources with memory, we observed that optimal prediction in the Wyner-Ziv regime is fundamentally different from that in non-distributed coding. That is because the prediction filters must not only jointly exploit the temporal and spatial redundancies, but the prediction filter of the source must also suppress the propagation of occasional decoding errors. At low rates, the optimal action turns out to be to allow more decoding errors but prevent their propagation aggressively using a very low prediction coefficient for the source. As the rate increases, it is more advantageous to allow less decoding errors and an increased prediction coefficient.

We also employed our scalar codes in transform coding with small block lengths (thereby achieving a low delay), where the source and side information are transformed separately. For the specific source-side information pairs studied, we showed that transform coding, even with a small block-length, outperforms predictive coding, despite the first-order Markov-like structure of the signals.

To keep our results in perspective, we also derived the asymptotic rate-distortion function for the special structure of sources we studied. Because we do not use the ideal Slepian-Wolf coding assumption anywhere in our results, the gap between the asymptotic rate-distortion function and performance of our schemes is more significant than usual.

Chapter 3

Zero-Delay Joint Source-Channel Coding for the Gaussian Wyner-Ziv Problem

3.1 Preliminary

Let's firstly review some fundamental estimation methods. It's well known that for an estimator to be unbiased we mean that *on the average* the estimator will yield the true value of the unknown parameter. Mathematically, if the true value is θ, an estimator is unbiased if $\mathbb{E}(\hat{\theta}) = \theta$. A natural optimality criterion for estimator is the *mean square error* (MSE), defined as $mse(\hat{\theta}) = \mathbb{E}\left[(\hat{\theta} - \theta)^2\right]$. The Cramer-Rao Lower Bound is one kind of method to find minimum variance unbiased (MVU) estimator. It is defined as below:

Theorem 15 *The variance of any unbiased estimator $\hat{\theta}$ must satisfy*

$$var(\hat{\theta}) \geq 1 \frac{1}{\mathbb{E}\left[\frac{\partial^2 lnp(x;\theta)}{\partial \theta^2}\right]}$$

Furthermore, if and only if

$$\frac{\partial ln(p(x;\theta)}{\partial \theta} = I(\theta)(g(x) - \theta)$$

the estimator, which is the MVU estimator, is $\hat{\theta} = g(x)$*, and the minimum variance is* $1/I(\theta)$.

However, MVU estimator usually is not easy to be found. In situations where the MVU estimator does not exist or cannot be found even if it exists, we use some other estimators to substitute. One of them is Maximum Likelihood Estimator(MLE), defined as the value of θ that maximizes the likelihood function. It could be found by taking the derivative of likelihood function or log-likelihood function and setting it to zero.

If we have available some prior knowledge about θ of interest, we wish to incorporate it into our estimator. So we need to assume that θ is a random variable with a given *prior* PDF. The Bayesian approach naturally allows us to make use of prior knowledge. Bayesian is also a good alternative estimator when an MVU estimator cannot be found. By assigning a PDF to θ we can try to find an estimator which is optimal "on the average" with respect to the assumed prior PDF of θ. In other words, we wish to find an estimator $\hat{\theta}$ that minimizes Bayesian MSE

$$Bmse(\hat{\theta}) = \int \left[\int (\theta - \hat{\theta})^2 p(\theta|x) d\theta \right] p(x) dx. \tag{3.1}$$

Taking the derivative of 3.1, we have

$$\frac{\partial}{\partial \hat{\theta}} \int (\theta - \hat{\theta})^2 p(\theta|x) d\theta = -2 \int \theta p(\theta|x) d\theta + 2\hat{\theta} \int p(\theta|x) d\theta$$

which when set equal to zero results in

$$\hat{\theta} = \mathbb{E}(\theta|x)$$

So the optimal estimator in terms of minimizing the Bayesian MSE is the mean of the *posterior* PDF $p(\theta|x)$. The posterior PDF refers to the PDF of θ *after* the data have been observed. Maximum a Posterior Estimator (MAP) refers to the estimator which

maximizes posterior function. In contrast, $p(\theta)$ or

$$p(\theta) = \int p(x, \theta) dx$$

may be thought of as the prior PDF of θ, indicating the PDF *before* the data are observed.

To calculate Posterior PDF then is important to either MAP estimation or MMSE estimation. Posterior PDF can be determined by Prior PDF and likelihood function through Bayes' rule.

$$\begin{aligned} p(\theta|x) &= \frac{p(x|\theta)p(\theta)}{p(x)} \\ &= \frac{p(x|\theta)p(\theta)}{\int p(x|\theta)p(\theta)d\theta} \end{aligned}$$

Note that the Bayesian philosophy to estimation has had a long and controversial history.

3.2 Introduction

In point to point communication with side information at the decoder, the simple analog scale-and-transmit scheme which is well known for its simplicity and optimality when Gaussian source transmitted over an additive white Gaussian noise (AWGN) channel [9], is no longer optimal one for a Gaussian source-channel pair. Now we know that the optimal distortion is:

$$D_{\text{opt}} = \frac{\sigma_N^2 \sigma_W^2}{P + \sigma_W^2}$$

$$D_{\text{analog}} = \frac{\sigma_N^2 \sigma_W^2}{P\sigma_N^2 + \sigma_W^2} > D_{\text{opt}}$$

As $\rho \to 1$, (i.e., $\sigma_N^2 \to 0$),

$$\frac{D_{\text{analog}}}{D_{\text{opt}}} = \frac{P + \sigma_W^2}{P\sigma_N^2 + \sigma_W^2} \to 1 + \frac{P}{\sigma_W^2}.$$

Separation principle still works, [10]. [7] and [8] both propose one kind of JSCC scheme to achieve optimal mean-squared error (MSE) distortion for the joint Wyner-Ziv

and dirty-paper coding. (If the channel interference is set to zero, the problem reduces to Wyner-Ziv coding which we are focusing on.) In the former one, Kochman etc used high-dimensional modulo-lattice modulation to quantize the source X, and then mapped the analog signal $X - Q(X)$ ($Q(X)$ is the output of quantizer) onto the channel. Wilson etc, [8], proposed with random coding arguments instead of lattice whereby the analog source is integrated into the random codeword.

In this chapter, we study the extreme of zero-delay hybrid digital/analog (HDA) schemes for the Wyner-Ziv setup, i.e., the joint source channel coding is to be done in a *scalar* fashion. One of the motivations for applying hybrid digital/analog (HDA) is that we could possibly mitigate the problem bringing by applying pure digital and pure analog systems, which includes that the performance of analog methods would change gradually with channel CSNR and the "threshold", "leveling-off" effects of digital modulation method. HDA transmission could help us achieve not only low delay, but also robustness to channel mismatch when CSI(channel state information) is unknown at the transmitter.

As we noticed, in [[7], Section V], the authors also discussed the low-delay scenario briefly without further investigation. They pointed out that the distortion grows fast in low dimensions due to the fact that enforcing a low probability of incorrect decoding results in a high loss factor. As we mentioned in chapter I, the coding scheme they used is actually a kind of analog mapping, (the output after applying a modulo-lattice modulation to the analog source). The channel input in our scheme is the superimposition of properly scaled quantized value (the digital component) and the quantization error (the analog component) after applying scalar quantization to the source.

We also numerically evaluate the robustness of two of the proposed schemes and compare them with that of purely analog transmission. Since in point to point communication, it is well known that separate source channel code is suboptimal to direct transmission of the source when channel SNR is unknown [31], it is meaningful to evaluate the performance of pure analog transmission in the presence of both channel SNR

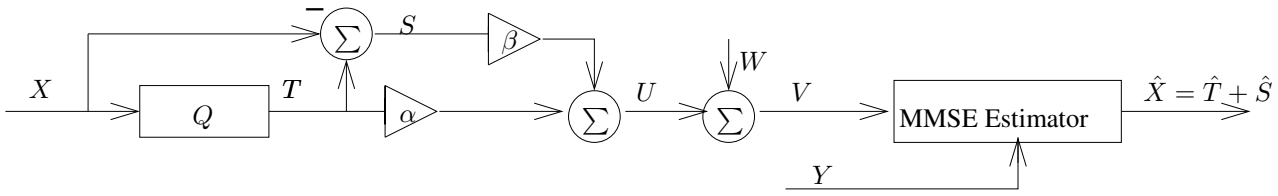

Figure 3.1: The proposed HDA Scalar Encoder with MMSE Estimator

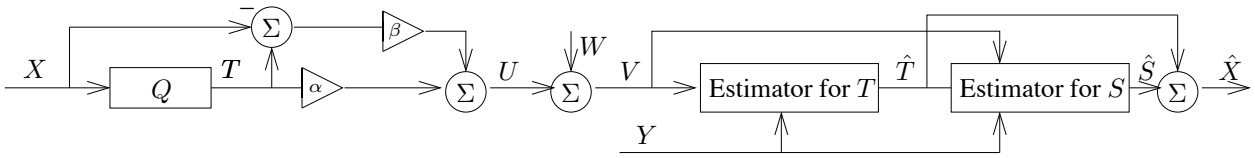

Figure 3.2: The proposed HDA Scalar Encoder with Sequential Estimator

and/or side information mismatch for comparison.

3.3 HDA Scalar Coding Scheme

Same with chapter II, we assume that the source-side information pair (X, Y) is jointly Gaussian with zero mean and covariance matrix

$$\begin{bmatrix} 1 & \rho \\ \rho & 1 \end{bmatrix}.$$

In other words, $X \sim \mathcal{N}(0,1)$ and

$$Y = \rho X + N$$

with $N \sim \mathcal{N}(0, \sigma_N^2)$ and $N \perp X$, where $\sigma_N^2 = 1 - \rho^2$. Source X is to be mapped to channel input U, which should satisfy the power constraint $\mathbb{E}[U^2] \leq P$. U then goes through an AWGN channel with additive noise $W \sim \mathcal{N}(0, \sigma_W^2)$ whose output is V. The source is to be reconstructed at the receiver which has access to both Y and V. Our proposed HDA encoder is shown as Fig.3.1 and Fig.3.2. The digital part is used to

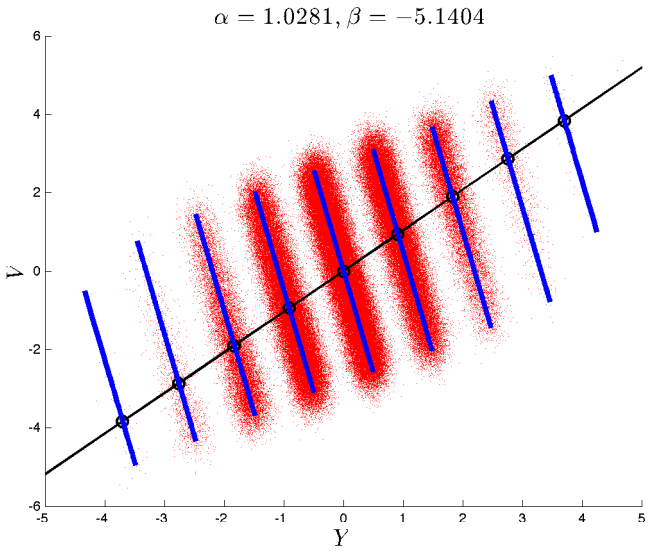

Figure 3.3: The distribution of points in the (Y, V)-plane. The sawtooth function indicates the channel input $U = \alpha T + \beta S$ against the "noise-free" side information ρX, while the straight line with equation $V = \frac{\alpha}{\rho} Y$ is shown to emphasize the effect of α. Circles on the latter correspond to $(\rho t_k, \alpha t_k)$.

transmit the quantized value $T = Q(X)$ produced by a regular scalar quantizer with reconstruction levels $\{r_k\}_{k=-\infty}^{\infty}$ and decision levels $\{d_k\}_{k=-\infty}^{\infty}$ with $d_{k-1} < r_k < d_k$. In parallel, the analog part is used to send the quantization error $S = X - T$. Then the scaled combination of T and S, $U = \alpha T + \beta S$, is sent through the AWGN channel at the output of which $V = U + W$ is observed.

Fig. 3.5 shows the distribution of $250,000$ (Y, V) pairs generated independently, as well as the sawtooth function indicating U as a function of ρX. The clearly visible "clusters" correspond to the reconstruction levels r_k, and the circles on the figure correspond to points $(\rho r_k, \alpha r_k)$, i.e., roughly the cluster centers, not corrupted by either the quantization error S or the noise pair (W, N). It is apparent that the decision levels should be far enough to ensure correct decoding of T with high enough probability. It should also be obvious that α and β must have opposite signs, because as the sawtooth climbs roughly along the line $V = \frac{\alpha}{\rho} Y$, which has positive slope, having β also positive would cause more overlap between the clusters. Therefore, in the rest of the paper, we assume $\alpha \geq 0$ and $\beta \leq 0$.

The optimal decoder for the proposed encoder, in the minimum MSE sense, is

$$\begin{aligned}\hat{X} &= \mathbb{E}[X|Y,V] \\ &= \mathbb{E}[T|Y,V] + \mathbb{E}[S|Y,V] \end{aligned} \tag{3.1}$$

3.3.1 HDA Encoder with MMSE Estimator

We can calculate the two terms in the equation (3.1) respectively, and the decoder model is shown as Fig.3.1.

$$\begin{aligned}\hat{r} &= \mathbb{E}[T|YV] \\ &= \sum_k r_k P_{T|YV}(r_k|y,v) \\ &= \frac{\sum_k \int_{d_{k-1}-r_k}^{d_k-r_k} r_k P_{TSYV}(r_k,s,y,v)ds}{\sum_k \int_{d_{k-1}-r_k}^{d_k-r_k} P_{TSYV}(r_k,s,y,v)ds} \\ &= \frac{\sum_k \int_{d_{k-1}-r_k}^{d_k-r_k} r_k P_{TS}(r_k,s)P_{YV|TS}(y,v|r_k,s)ds}{\sum_k \int_{d_{k-1}-r_k}^{d_k-r_k} P_{TS}(r_k,s)P_{YV|TS}(y,v|r_k,s)ds} \\ &= \frac{\sum_k \int_{d_{k-1}-r_k}^{d_k-r_k} r_k P_X(r_k+s)P_N(y-\rho r_k-\rho s)P_W(v-\alpha r_k-\beta s)ds}{\sum_k \int_{d_{k-1}-r_k}^{d_k-r_k} P_X(r_k+s)P_N(y-\rho r_k-\rho s)P_W(v-\alpha r_k-\beta s)ds}\end{aligned}$$

Defining

$$\sigma^2 = \frac{\sigma_N^2\sigma_W^2}{\sigma_W^2+\beta^2\sigma_N^2}$$

and

$$\begin{aligned}\mu_k(y,v) &= \frac{\rho\sigma_W^2(y-\rho r_k)+\beta\sigma_N^2(v-\alpha r_k)-\sigma_N^2\sigma_W^2 r_k}{\sigma_W^2+\beta^2\sigma_N^2} \\ &= \frac{\rho\sigma_W^2 y+\beta\sigma_N^2 v - r_k(\sigma_W^2+\alpha\beta\sigma_N^2)}{\sigma_W^2+\beta^2\sigma_N^2}\,,\end{aligned}$$

we can proceed as

$$\hat{r} = \frac{\sum_k r_k\left[\mathrm{erf}\left(\frac{d_k-r_k-\mu_k(y,v)}{\sigma\sqrt{2}}\right)-\mathrm{erf}\left(\frac{d_{k-1}-r_k-\mu_k(y,v)}{\sigma\sqrt{2}}\right)\right]\cdot\exp(A)}{\sum_k\left[\mathrm{erf}\left(\frac{d_k-r_k-\mu_k(y,v)}{\sigma\sqrt{2}}\right)-\mathrm{erf}\left(\frac{d_{k-1}-r_k-\mu_k(y,v)}{\sigma\sqrt{2}}\right)\right]\cdot\exp(A)}$$

where

$$\begin{aligned} A &= -\frac{1}{2\sigma_N^2\sigma_W^2}\big(\sigma_N^2\sigma_W^2 r_k^2 + \sigma_W^2(y-\rho r_k)^2 + \sigma_N^2(v-\alpha r_k)^2 \\ &- \frac{\left[\rho\sigma_W^2 y + \beta\sigma_N^2 v - r_k(\sigma_W^2 + \alpha\beta\sigma_N^2)\right]^2}{\sigma_W^2 + \beta^2\sigma_N^2}\big) \end{aligned}$$

And for the estimation of S, we have

$$\begin{aligned} \hat{S} &= E[S|V=v, Y=y] \\ &= \int_{-\infty}^{\infty} sP_{S|VY}(s|v,y)ds \\ &= \frac{\int_{-\infty}^{\infty} sP_{SVY}(s,v,y)ds}{P_{VY}(v,y)} \\ &= \frac{\sum_k \int_{d_{k-1}-r_k}^{d_k-r_k} sP_X(r_k+s)P_N(y-\rho r_k-\rho s)P_W(v-\alpha r_k-\beta s)ds}{\sum_k \int_{d_{k-1}-r_k}^{d_k-r_k} P_X(r_k+s)P_N(y-\rho r_k-\rho s)P_W(v-\alpha r_k-\beta s)ds} \\ &= \frac{\sum_k \exp\left[-\frac{1}{2\sigma^2}(-\mu_k^2 + \frac{\sigma_N^2\sigma_W^2 r_k^2 + \sigma_W^2(y-\rho r_k)^2 + \sigma_N^2(v-\alpha r_k)^2}{\sigma_W^2+\sigma_N^2\beta^2})\right]\left[\sigma^2 B_k + \mu_k \times \frac{\sqrt{2\pi}\sigma}{2} \times C_k\right]}{\sum_k \exp\left[-\frac{1}{2\sigma^2}(-\mu_k^2 + \frac{\sigma_N^2\sigma_W^2 r_k^2 + \sigma_W^2(y-\rho r_k)^2 + \sigma_N^2(v-\alpha r_k)^2}{\sigma_W^2+\sigma_N^2\beta^2})\right] \times \frac{\sqrt{2\pi}\sigma}{2} \times C_k} \end{aligned}$$

where

$$\begin{aligned} B_k &= \exp\left[-\frac{1}{2\sigma^2}(d_{k-1}-r_k-\mu_k)^2\right] - \exp\left[-\frac{1}{2\sigma^2}(d_k-r_k-\mu_k)^2\right] \\ C_k &= \operatorname{erf}\left(\frac{d_k-r_k-\mu_k}{\sigma\sqrt{2}}\right) - \operatorname{erf}\left(\frac{d_{k-1}-r_k-\mu_k}{\sigma\sqrt{2}}\right) \end{aligned}$$

3.3.2 HDA Encoder with Sequential Estimator

(3.1) is too complicated to be expressed in closed form. To simplify it, we propose two suboptimal schemes, in each of which the decoder first estimates T using a MAP estimator, and then optimally estimates S assuming that $\hat{T}$, the estimate of T, is correct. The decoder scheme is illustrated in Fig.3.2. This setting creates tension between α and β: We need large α to increase the probability of correctly decoding T, and we need large β to estimate S accurately, while satisfying the power constraint.

3.3.2.1 Scheme A

The MAP estimator is given by $\hat{T}(y,v) = r_{k^*}$ where

$$\begin{aligned}
k^* &= \arg\max_k P_{TYV}(r_k, y, v) \\
&= \arg\max_k \int_{d_{k-1}-r_k}^{d_k-r_k} P_{TSYV}(r_k, s, y, v)ds \\
&= \arg\max_k \int_{d_{k-1}-r_k}^{d_k-r_k} P_{TS}(r_k, s)P_{YV|TS}(y, v|r_k, s)ds \\
&= \arg\max_k \int_{d_{k-1}-r_k}^{d_k-r_k} P_T(r_k)P_{S|T}(s|r_k)P_{Y|TS}(y|r_k, s) \\
&\qquad \cdot P_{V|TS}(v|r_k, s)ds \\
&= \arg\max_k \int_{d_{k-1}-r_k}^{d_k-r_k} P_X(r_k + s)P_N(y - \rho r_k - \rho s) \\
&\qquad \cdot P_W(v - \alpha r_k - \beta s)ds \\
&= \arg\max_k \int_{d_{k-1}-r_k}^{d_k-r_k} \exp\left[-\frac{1}{2\sigma_N^2\sigma_W^2}\left\{ s^2(\sigma_W^2 + \beta^2\sigma_N^2) \right.\right. \\
&\quad -2s\left(\rho\sigma_W^2(y - \rho r_k) + \beta\sigma_N^2(v - \alpha r_k) - \sigma_N^2\sigma_W^2 r_k\right) \\
&\quad \left.\left. +\sigma_N^2\sigma_W^2 r_k^2 + \sigma_W^2(y - \rho r_k)^2 + \sigma_N^2(v - \alpha r_k)^2 \right\}\right] ds \ .
\end{aligned}$$

Defining

$$\sigma^2 = \frac{\sigma_N^2\sigma_W^2}{\sigma_W^2 + \beta^2\sigma_N^2}$$

and

$$\begin{aligned}
\mu_k(y, v) &= \frac{\rho\sigma_W^2(y - \rho r_k) + \beta\sigma_N^2(v - \alpha r_k) - \sigma_N^2\sigma_W^2 r_k}{\sigma_W^2 + \beta^2\sigma_N^2} \\
&= \frac{\rho\sigma_W^2 y + \beta\sigma_N^2 v - r_k(\sigma_W^2 + \alpha\beta\sigma_N^2)}{\sigma_W^2 + \beta^2\sigma_N^2},
\end{aligned}$$

we can proceed as in (3.2), where in the last two steps, we used the fact that terms that do not depend on k do not change the maximum.

$$
\begin{aligned}
k^* &= \arg\max_k \int_{d_{k-1}-r_k}^{d_k-r_k} \exp\Bigg[-\frac{1}{2\sigma^2}\Bigg\{ \Big(s-\mu_k\Big)^2 - \mu_k^2 \\
&\quad + \frac{\sigma_N^2\sigma_W^2 r_k^2 + \sigma_W^2(y-\rho r_k)^2 + \sigma_N^2(v-\alpha r_k)^2}{\sigma_W^2+\beta^2\sigma_N^2} \Bigg\}\Bigg] ds \\
&= \arg\max_k \Bigg\{ \left[\operatorname{erf}\left(\frac{d_k - r_k - \mu_k}{\sigma\sqrt{2}}\right) - \operatorname{erf}\left(\frac{d_{k-1} - r_k - \mu_k}{\sigma\sqrt{2}}\right)\right] \\
&\quad \cdot \exp\Big[-\frac{1}{2\sigma_N^2\sigma_W^2}\Bigg\{ \left(\sigma_W^2 + \alpha^2\sigma_N^2 - \frac{(\sigma_W^2+\alpha\beta\sigma_N^2)^2}{\sigma_W^2+\beta^2\sigma_N^2}\right) r_k^2 \\
&\quad -2\left(\sigma_W^2 y\rho + \sigma_N^2 v\alpha - \frac{(\sigma_W^2+\alpha\beta\sigma_N^2)(\rho\sigma_W^2 y + \beta\sigma_N^2 v)}{\sigma_W^2+\beta^2\sigma_N^2}\right) r_k \Bigg\}\Big]\Bigg\} \\
&= \arg\max_k \Bigg\{ \left[\operatorname{erf}\left(\frac{d_k - r_k - \mu_k}{\sigma\sqrt{2}}\right) - \operatorname{erf}\left(\frac{d_{k-1} - r_k - \mu_k}{\sigma\sqrt{2}}\right)\right] \\
&\quad \cdot \exp\left[-\frac{1}{2(\sigma_W^2+\beta^2\sigma_N^2)} \{v - \rho\beta y - (\alpha-\beta) r_k\}^2 \right] \Bigg\} \qquad (3.2)
\end{aligned}
$$

Now, for the optimal estimation of S (conditioned on $T = r_{k^*}$), we have

$$
\begin{aligned}
\hat{S} &= E[S|V=v, Y=y, T=r_{k^*}] \\
&= \int_{d_{k^*-1}-t_{k^*}}^{d_{k^*}-t_{k^*}} s P_{S|VYT}(s|v,y,r_{k^*}) ds \\
&= \int_{d_{k^*-1}-t_{k^*}}^{d_{k^*}-t_{k^*}} s \frac{P_{S|T}(s|r_{k^*}) P_{VY|ST}(v,y|s,r_{k^*})}{P_{VY|T}(v,y|r_{k^*})} ds \\
&= \frac{\int_{d_{k^*-1}-t_{k^*}}^{d_{k^*}-t_{k^*}} s P_{S|T}(s|r_{k^*}) P_{VY|ST}(v,y|s,r_{k^*}) ds}{\int_{d_{k^*-1}-t_{k^*}}^{d_{k^*}-t_{k^*}} P_{S|T}(s|r_{k^*}) P_{VY|ST}(v,y|s,r_{k^*}) ds} \\
&= \frac{\int_{d_{k^*-1}-t_{k^*}}^{d_{k^*}-t_{k^*}} s P_X(r_{k^*}+s) P_W(w) P_N(n) ds}{\int_{d_{k^*-1}-t_{k^*}}^{d_{k^*}-t_{k^*}} P_X(r_{k^*}+s) P_W(w) P_N(n) ds} \qquad (3.3)
\end{aligned}
$$

where $w = v - \alpha r_{k^*} - \beta s$ and $n = y - \rho r_{k^*} - \rho s$. Using the same algebra as before, and canceling all the terms independent of s, (3.3) can be reduced to

$$
\begin{aligned}
\hat{S} &= \frac{\int_{d_{k^*-1}-t_{k^*}}^{d_{k^*}-t_{k^*}} s \exp\left[-\frac{1}{2\sigma^2}(s-\mu_{k^*})^2\right] ds}{\int_{d_{k^*-1}-t_{k^*}}^{d_{k^*}-t_{k^*}} \exp\left[-\frac{1}{2\sigma^2}(s-\mu_{k^*})^2\right] ds} \\
&= \mu_{k^*} + \sqrt{\frac{2\sigma^2}{\pi}} \cdot \frac{\int_l^u 2z\exp(-z^2) dz}{\operatorname{erf}(u) - \operatorname{erf}(l)}, \qquad (3.4)
\end{aligned}
$$

where $u = \frac{d_{k^*} - r_{k^*} - \mu_{k^*}}{\sigma\sqrt{2}}$, $l = \frac{d_{k^*-1} - r_{k^*} - \mu_{k^*}}{\sigma\sqrt{2}}$.

The distortion achieved by the proposed HDA encoder and decoder seems to be very difficult to derive in a closed form. Instead, we obtain it by numerical simulation.

3.3.2.2 Scheme B

Notice that the difficulty in an analytical derivation of the distortion in Scheme A mainly stems from the first step of the decoder. It is not clear how incorrect decoding of T affects the resultant distortion. We propose a remedy to this problem, and propose a simplified scheme. In this scheme, at the decoder, the (Y, V) pair is first normalized and rotated so that

$$\begin{aligned}
&\begin{bmatrix} Z_1 \\ Z_2 \end{bmatrix} \\
&= \sqrt{\frac{\sigma_W^2\sigma_N^2}{\beta^2\sigma_N^2+\rho^2\sigma_W^2}} \begin{bmatrix} -\beta/\sigma_W & \rho/\sigma_N \\ -\rho/\sigma_N & -\beta/\sigma_W \end{bmatrix} \begin{bmatrix} Y/\sigma_N \\ V/\sigma_W \end{bmatrix} \\
&= \frac{1}{\sqrt{\beta^2\sigma_N^2+(1-\sigma_N^2)\sigma_W^2}} \begin{bmatrix} \rho V-\beta Y \\ -\beta\frac{\sigma_N}{\sigma_W}V-\rho\frac{\sigma_W}{\sigma_N}Y \end{bmatrix} \\
&= \begin{bmatrix} cT+N_1' \\ aT+bS+N_2' \end{bmatrix}
\end{aligned}$$

where

$$\begin{aligned}
a &= -\frac{\alpha\beta\sigma_N^2+(1-\sigma_N^2)\sigma_W^2}{\sigma_W\sigma_N\sqrt{\beta^2\sigma_N^2+(1-\sigma_N^2)\sigma_W^2}} \\
b &= -\frac{\sqrt{\beta^2\sigma_N^2+(1-\sigma_N^2)\sigma_W^2}}{\sigma_W\sigma_N} \\
c &= \frac{\rho(\alpha-\beta)}{\sqrt{\beta^2\sigma_N^2+(1-\sigma_N^2)\sigma_W^2}} \\
N_1' &= \frac{\rho W-\beta N}{\sqrt{\beta^2\sigma_N^2+(1-\sigma_N^2)\sigma_W^2}} \\
N_2' &= \frac{-\beta\sigma_N^2 W-\rho\sigma_W^2 N}{\sigma_W\sigma_N\sqrt{\beta^2\sigma_N^2+(1-\sigma_N^2)\sigma_W^2}}\,.
\end{aligned}$$

Note that the covariance matrix of the jointly Gaussian pair (N_1', N_2') is $\mathbf{I}$.

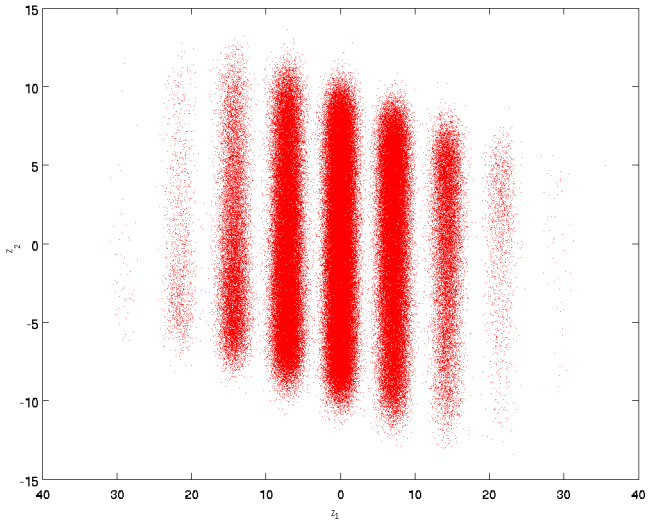

Figure 3.4: The distribution of points in the (Z_1, Z_2)-plane.

At this point, we observe that if the quantizer meets the centroid condition, i.e.,

$$\mathbb{E}[S|T] = 0 \ ,$$

then Z_1 is *uncorrelated* with S. Motivated by this, we enforce the centroid condition (regardless of whether the decision levels are uniformly or non-uniformly spaced), and first decode T using only Z_1. Then assuming T is correctly decoded, we decode S using only $Z_2 - a\hat{T}$.

Now, decoding T using a MAP estimator yields

$$k^* = \arg\max_k p_k e^{-(z_1 - cr_k)^2/2}$$

where $p_k = \Pr[T = r_k]$. If we further assume that the decision boundary q_k between $T = r_k$ and $T = r_{k+1}$ is always in the interval (cr_k, cr_{k+1}), then q_k must satisfy

$$p_k e^{-(q_k - cr_k)^2/2} = p_{k+1} e^{-(q_k - cr_{k+1})^2/2}$$

and thus

$$q_k = \frac{c(r_k + r_{k+1})}{2} + \frac{1}{c(r_{k+1} - r_k)} \ln \frac{p_k}{p_{k+1}} \ .$$

Also assume that c is high enough to ensure that if $T = r_k$, then $\hat{T}$ is either one of r_{k-1}, r_k, or r_{k+1}. From this assumption, $E[(T - \hat{T})^2]$ can be written in closed form as

a summation over k.

$$\begin{aligned}
&\mathbb{E}[(T-\hat{T})^2] \\
&= \mathbb{E}[(T-\hat{T})^2 | T \neq \hat{T}] P(T \neq \hat{T}) \\
&= \sum_k \Big[(r_k - r_{k-1})^2 P_{T,\hat{T}}(t = r_k, \hat{t} = r_{k-1}) \\
&\qquad + (r_k - r_{k+1})^2 P_{T,\hat{T}}(t = r_k, \hat{t} = r_{k+1}) \Big] \\
&= \sum_k (r_k - r_{k-1})^2 P_T(t = r_k) \\
&\cdot \quad \Big[P_{N_1'}(n_1' < q_{k-1} - c r_k) + P_{N_1'}(n_1' > q_k - c r_k) \Big]
\end{aligned}$$

Once $\hat{T}$ is found, S is estimated in a linear fashion from $Z_2 - a\hat{T}$, i.e.,

$$\hat{S} = d(Z_2 - a\hat{T}) \; .$$

Ignoring decoding errors in T, the optimal linear coefficient is given by

$$d = \frac{b\sigma_S^2}{b^2\sigma_S^2 + 1} \; .$$

Now, the overall distortion becomes

$$\begin{aligned}
D &= E[(T + S - \hat{T} - \hat{S})^2] \\
&= E[(T + S - \hat{T} - d(Z_2 - a\hat{T}))^2] \\
&= E[(T + S - \hat{T} - d(aT + bS + N_2' - a\hat{T}))^2] \\
&= E\left[\Big((1-ad)(T - \hat{T}) + (1-bd)S - dN_2' \Big)^2 \right] \\
&= (1-ad)^2 E[(T-\hat{T})^2] + (1-bd)^2 \sigma_S^2 + d^2 \\
&\qquad -2(1-ad)(1-bd) E[S\hat{T}] \\
&= (1-ad)^2 E[(T-\hat{T})^2] + \frac{\sigma_S^2}{b^2\sigma_S^2 + 1} \qquad (3.5)
\end{aligned}$$

where, the last line follows the fact that S and $\hat{T}$ are uncorrelated. That in turn is

because

$$\begin{aligned}
& E[S\hat{T}] \\
= & \sum_k p_k E[S\hat{T}|T=r_k] \\
= & \sum_k p_k \int_{d_{k-1}-r_k}^{d_k-r_k} \sum_l s r_l p_{S|T}(s|r_k) p_{\hat{T}|ST}(r_l|s,r_k) ds \\
\overset{(a)}{=} & \sum_k p_k \int_{d_{k-1}-r_k}^{d_k-r_k} \sum_l s r_l p_{S|T}(s|r_k) p_{\hat{T}|T}(r_l|r_k) ds \\
= & \sum_k p_k E[S|T=r_k] E[\hat{T}|T=r_k] \\
\overset{(b)}{=} & 0
\end{aligned}$$

where (a) follows from the fact that $\hat{T}$ does not depend on S when T is given, and (b) follows from the centroid condition.

3.3.3 Scheme C: HDA coding with pseudo-binning

For uniform quantization, instead of sending $U = \alpha T + \beta S$, send $U = \tilde{T} + \beta S$, where

$$\tilde{T} = \text{mod}\left[\alpha\frac{T}{\Delta} + \frac{\Sigma}{2}, \Sigma\right] - \frac{\Sigma}{2}$$

3.4 Simulation Results

3.4.1 Transmission Under Known Channel and Side Information Quality

A performance comparison is shown in Fig.3.7 assuming $\sigma_W^2 = 0.1$. Fig.3.7 (a), (b), and (c) represent different correlation values ρ between X and Y. The following schemes are included in the comparison:

- HDA encoder with MMSE estimator: The results shown on the figure are obtained

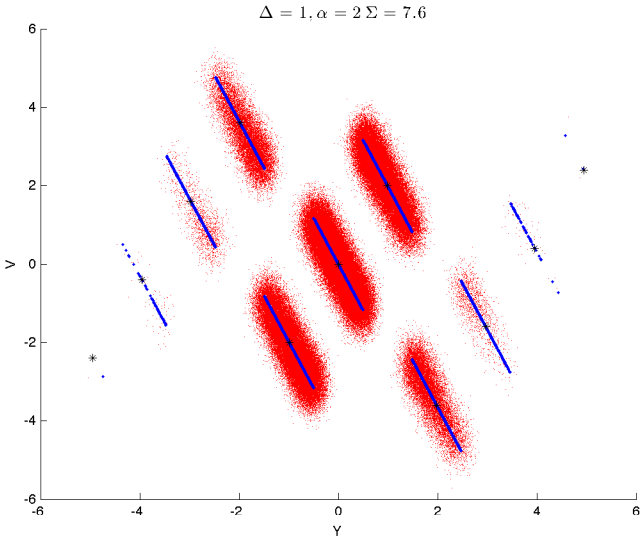

Figure 3.5: The distribution of points in the (Y, V)-plane when U now equals $\tilde{T}_\beta S$.

by numerical simulation, whereby $1,000,000$ independent (X, Y, W) triplets are generated.

- HDA scheme A: The results shown on the figure are obtained by numerical simulation, whereby $1,000,000$ independent (X, Y, W) triplets are generated. Although the centroid condition is not crucial for the derivation of the estimators here, it will minimize the variance of S for given decision levels, and hence is still adopted.

- HDA scheme B: The results shown on the figure are obtained using the analytical distortion formula (3.5). We also observed by numerical simulations that the formula is accurate when the quantizer resolution is low enough, which we enforced.

- HDA scheme B with $\alpha = 0$: The input of the channel is the analog signal βS. The same decoder in scheme B is used at the receiver.

- Kochman encoder with sequential estimator B: when dimension of lattice quantizer in [7] comes to 1, the encoder model could be shown as Fig. 3.6.

- Pure analog scheme: This is the classical analog scale-and-transmission scheme.

- Pure digital scheme: Using Scheme C, when $\beta = 0$ and α is submultiple of Σ.

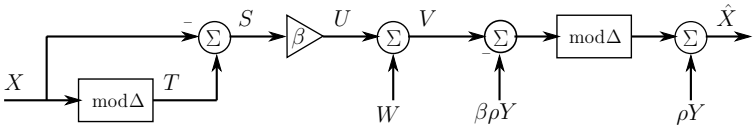

Figure 3.6: Kochman's Encoder Model when dimension comes to 1.

- Iterative Mapping Scheme Proposed by Emrah when $\rho = 0.9$.

For the first three cases above, we varied parameters α, β, and Δ (the uniform spacing of decision levels) under the power constraint to find the optimal results, and for the fourth one, we varied only β and Δ. Since α is fixed to be zero, the optimal performance is always worse than that of HDA scheme B. In fact, the performance of this scheme almost coincides with that of pure analog coding for low and moderate correlation values. The HDA encoder with MMSE estimator performances best as expected. We also observe that scheme A is superior to scheme B, as in the former, we estimate T with jointly using Y and V, while in the latter, T is decoded using one dimensional data. However, the gap seems to be small for all correlation levels. While $\rho = 0.9$, [34] gave the SNR results by their algorithm. It could be seen in (3.7)(b), our scheme gain almost as high as 0.5dB advantage by theirs. Compared with all the schemes except pure digital one, the pure analog scheme yields the worst performance as expected, and the larger the correlation, the larger the gap between the HDA scenarios and the pure analog scheme. Pure digital one beats pure analog one only when correlation is as high as 0.99. For the scheme with MMSE estimator and scheme B, the optimized combinations of α, β, Δ in different cases of ρ when $CSNR = 14.7712dB$ are illustrated in Table 3.1 and Table 3.2 respectively. Optimal Δ increases with the decreasing of correlation between source and side information. In fact, we also observed that when ρ is as low as 0.8, Δ becomes very large, thereby reducing the HDA schemes to pure analog transmission. This explains why the gap between the HDA schemes and analog transmission shrinks as ρ decreases.

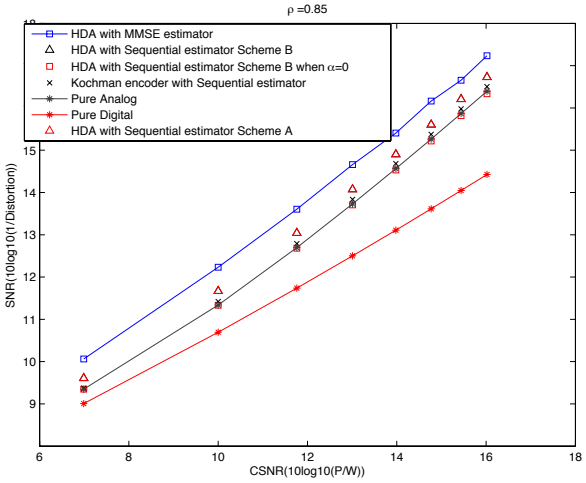

(a)

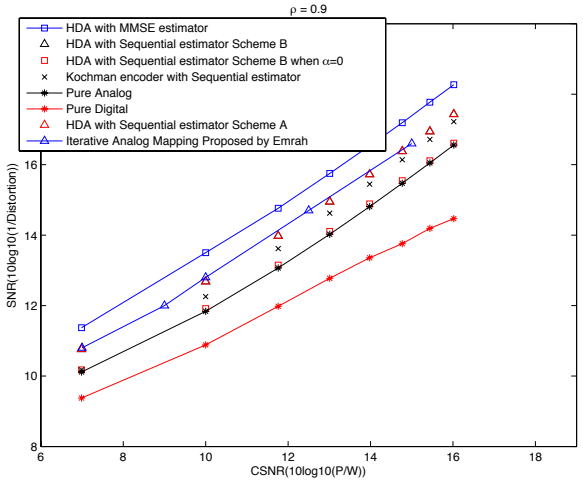

(b)

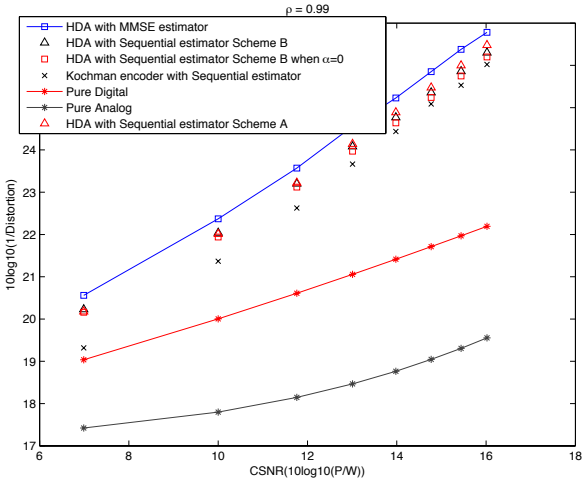

(c)

Figure 3.7: Comparison of the Channel SNR - Source SNR performance for various Schemes

Table 3.1: Optimized Parameters for the Scheme with MMSE estimator

	Δ	α	β
$\rho = 0.85$	3.1778	0.6576	-2.2675
$\rho = 0.90$	2.5566	0.7576	-2.6345
$\rho = 0.99$	1.04	0.34	-5.9166

Table 3.2: Optimized Parameters for Scheme B.

	Δ	α	β
$\rho = 0.85$	4.8980	1.2634	-1.7816
$\rho = 0.90$	3.6550	1.1831	-1.9497
$\rho = 0.99$	1.0424	0.5265	-5.7510

3.4.2 Transmission Under Uncertainty Conditions

We now experimentally evaluate the performance of the HDA scheme B when the variance of the channel noise W and/or the noise power σ_N^2 at the side information "channel" (equivalently the correlation ρ) mismatch the values assumed during encoder design. Since pure analog transmission is completely robust to channel SNR mismatch when there is no side information, we also evaluate its performance in the presence of side information mismatch for comparison.

In our experiment, we designed our encoder for the parameters $\rho = 0.99$, $CSNR \approx 14.77$, and varied (ρ, σ_W^2) in a range around the pair $(0.99, 0.1)$. The decoder is assumed to know the (ρ, σ_W^2) perfectly. Fig. 3.8 compares the resultant performances of the HDA scheme B and the purely analog scheme against the Wyner-Ziv bound. It is clear that the HDA scheme is more sensitive to a decrease in ρ than the purely analog scheme. That is expected, because correct decoding of T depends on a good enough spacing (with respect to σ_N) between the reconstruction values of the quantizer, and incorrect decoding of T, though not catastrophic, would rapidly affect the distortion. On the other hand, in the range where the mismatch of ρ is still tolerable, it seems that the HDA scheme B continues to be superior to pure analog transmission under channel SNR mismatch.

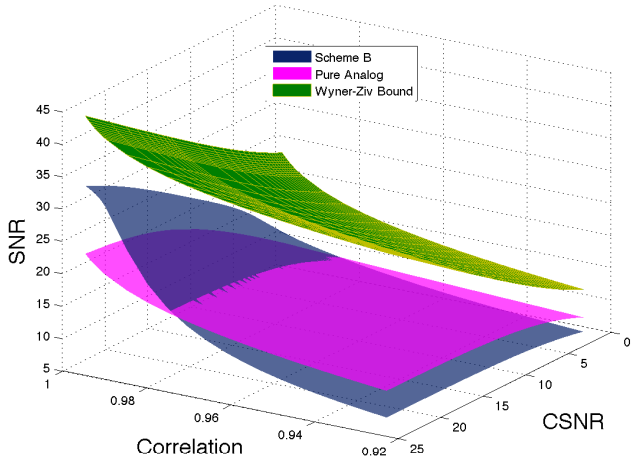

Figure 3.8: Performance of schemes under mismatch.

Chapter 4

Low Delay Coding for Channel Bandwidth Expansion Problem

4.1 Introduction

The JSCC WZ problem is intimately related with JSCC without side information but with bandwidth expansion factor 2. In [31], the author generalized a class of analog codes which mapped the source message x into a sequence $u[n]$ of length N, where N is bandwidth expansion factor. In detail, the message x is embedded in an initial state variable $z[0]$, and the corresponding encoding $u[0], u[1], ..., u[N-1]$ is obtained via iterations of the dynamical system

$$\begin{aligned} z[n+1] &= f(z[n]) \qquad z[0] = x \\ u[n] &= g(z[n]) \end{aligned}$$

where f is the iteration function with dynamic system and g is appropriate observation function corresponding to specific f. Particularly, the authors developed an efficient JSCC code with tent mapping and a fast decoding algorithm. As we noted in the first sentence of this paragraph, when $N = 2$, chen's work could be viewed as designing JSCC

code while transmission of $u[2]$ viewed previous one $u[1]$ as Wyner-Ziv side information. However, the source he applied the algorithm on is distributed uniformly on $[-1, 1]$ instead of Gaussian source so that no matter how the dynamical system iterates, the value of the sequence would be constrained in the interval $[-1, 1]$.

Another interesting JSCC mapping for 1 to 2 channel expansion problem is inverse spiral mapping [32],[33]. The detailed mapping scheme would be described in the next section.

[34] proposed an iterative algorithm to obtain the optimal map between the $m-$dimensional source space and $n-$ dimensional channel space. Since the iterative algorithm updates encoder and decoder mappings according to necessary condition for optimality, the initial mapping is of great importance, otherwise, the search of optimal mapping could easily stop when distortion reaches a local minimum which is far from global one.

In this chapter, we will discuss the scheme that integrates our HDA encoder into channel bandwidth expansion problem. Specifically, when bandwidth expansion factor is 2, the source message X is mapped onto $2-$dimensional channel input U_1 and U_2 within power constraint $\mathbb{E}[U_1^2] + \mathbb{E}[U_2^2] \leq P$. Then U_1, U_2 are transmitted either through an AWGN channel sequentially or through two AWGN channel respectively. Here we assume the case is former one. The Gaussian noise W_1 and W_2 with zero mean and variance σ_W^2 are assumed to be independent of the signal. At the decoder part, we could reconstruct X by mapping $2-$dimensional channel output $V_1 = U_1 + W_1$ and $V_2 = U_2 + W_2$ to $\hat{X}$.

4.2 Two Low-Delay Coding Scheme proposed for 1:2 Source-Channel Space Mapping

4.2.1 HDA Encoder Combined with Inverse Spiral Mapping

Firstly, let's review the inverse spiral mapping scheme. With inverse spiral mapping, each source symbol x is mapped to the corresponding point on Archimedean bi-spiral which is with rectangular coordinate values (u_1, u_2) or with polar coordinate values $(\rho = x, \theta = x)$. In other words, the analog signal is modulated on a spiral in the two dimensional plane.

$$\begin{aligned} u_1 &= x\cos x \\ u_2 &= \begin{cases} x\sin x & x \geq 0, \\ -x\sin x & x < 0. \end{cases} \end{aligned}$$

At the decoder part, given channel outputs (V_1, V_2) we could find the corresponding point V on the coordinate plane. You can see from Fig. **??** that due to the interruption of channel noise, the point corresponding output from channel is now the red one while the point corresponding to true value is shown as the black one.

[32] introduced M.L. estimator for inverse spiral mapping. The M.L. estimator in a Gaussian noise is the minimum Euclidean distance estimator. The estimator tries to find the point on the bi-spiral which is closest to the point V. [32] gave a simplified high SNR approximation of M.L. estimator, proved its effectiveness by comparison with CRLB and compared the performance of inverse spiral coding with tent map coding when the source is also uniformly distributed in $[-1, 1]$.

In [33], the authors proposed to use Archimedes' spiral as a $2:1$ bandwidth reducing mapping for transmission of $2-$*dimensional* Gaussian sources.

The spiral mapping is inherently based on the idea that we should occupy the power space efficiently. In other words, we use less power to transmit the source message closer to original point (for Gaussian source, i.e., the source message with higher probability)

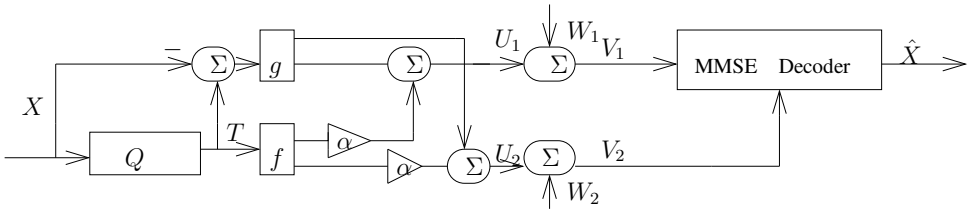

Figure 4.1: The Model of Scheme A

while using more power to transmit the source message further from original point (for Gaussian source, i.e., with less probability). In chapter III, it reveals that one of the facts that effect the performance of hybrid digital and analog mapping in the presence of side information is the distribution of those blue lines on the $Y - V$ plane. The conclusions above inspire us to distribute these blue lines along the spiral.

Given gaussian source X, by a uniform scalar quantizer Q with reconstruction levels $\{r_k\}_{k=-\infty}^{\infty}$ and decision levels $\{d_k\}_{k=-\infty}^{\infty}$ with $r_k = \frac{d_k + d_{k-1}}{2}$, we obtain digital component $T = Q(X)$ and analog component $S = X - T$. Define $k = \frac{T}{\Delta}$. Then channel inputs U_1, U_2 are defined as

$$\begin{aligned} \begin{bmatrix} U_1 \\ U_2 \end{bmatrix} &= \alpha f(T) + g(S) \\ &= \alpha \begin{bmatrix} x' \\ y' \end{bmatrix} + g(S) \end{aligned}$$

where $1:2$ mapping f maps T onto a point with rectangular coordinate value (x', y')on the spiral. The point could be alternatively expressed by (θ, θ) in polar coordinates or by (x', y') in rectangular coordinates. The mapping rule is illustrated below:

- when $k = 0$, $\theta_0 = 0$, i.e., $x'_0 = 0, y'_0 = 0$;
- when $k = 1$, θ_1 should be the minimum positive value which satisfies the equation $\frac{\sin\theta + \theta\cos\theta}{\cos\theta - \theta\sin\theta} = 0$, (the reason would be revealed later), then $x'_1 = \theta_1 \cos\theta_1$, $y' = \theta_1 \sin\theta_1$.

- when $k = -1$, θ_{-1} should be the maximum negative value which satisfies the equation $-\frac{\sin\theta+\theta\cos\theta}{\cos\theta-\theta\sin\theta} = 0$, then $x'_{-1} = \theta_{-1}\cos\theta_{-1}$, $y' = -\theta_{-1}\sin\theta_{-1}$.

- when $k > 1$, the points representing $f(T)$ are distributed on the uni-positive-spiral with approximate equal distance along the spiral. Use parameter l to represent the distance. Then $l \approx \frac{1}{2}(\theta_k + \theta_{k-1})(\theta_k - \theta_{k-1})$. So $\theta_k = \sqrt{\theta_1^2 + 2(k-1)l}$, $x'_k = \theta_1\cos\theta_1$, $y'_k = \theta_1\sin\theta_1$.

- when $k < -1$, the points representing $f(T)$ are distributed on the uni-negative-spiral with approximate equal distance along the spiral. Similarly $l \approx \frac{1}{2}(\theta_k + \theta_{k-1})(\theta_k - \theta_{k-1})$. So $\theta_k = -\sqrt{\theta_{-1}^2 - 2(k+1)l}$, $x'_k = \theta_1\cos\theta_1$, $y'_k = -\theta_1\sin\theta_1$.

To analog component S, once k is determined by $k = \frac{T}{\Delta}$,

$$g(S) = \begin{bmatrix} \beta_{1k}S \\ \\ \beta_{2k}S \end{bmatrix},$$

where, β_{1k} and β_{2k} are fixed parameters for determined k. Note that for $k = \frac{T}{\Delta}$, T is mapped to point (x', y'), then the slope of tangent line to the spiral at the point (x', y') is $\mathrm{sgn(k)}\frac{\sin\theta+\theta\cos\theta}{\cos\theta-\theta\sin\theta}$. Define the length of the blue line corresponding to determined k is c, then, obviously, $c = \Delta\sqrt{(}\beta_{1k}^2+\beta_{2k}^2)$. Then β_{1k} and β_{2k} could be found by the equation groups. The whole encoder-decoder scheme could be shown in Fig. .

$$\begin{aligned} \frac{\beta_{2k}}{\beta_{1k}} &= \mathrm{sgn(k)}\frac{\sin\theta+\theta\cos\theta}{\cos\theta-\theta\sin\theta} \\ c &= \Delta\sqrt{(}\beta_{1k}^2+\beta_{2k}^2) \end{aligned}$$

The distribution of points in the $U_1 - U_2$ plane can be shown in Figure. .

4.2.2 HDA Encoder with "Side information"

In chapter III, we plot $2-$dimensional $Y - V$ plane, which could be naturally viewed as $2-$dimensional $V_1 - V_2$ space. Hereby, Y is no longer side information but the output of channel V_1. Recall the conception of "side information channel" that Y is generated

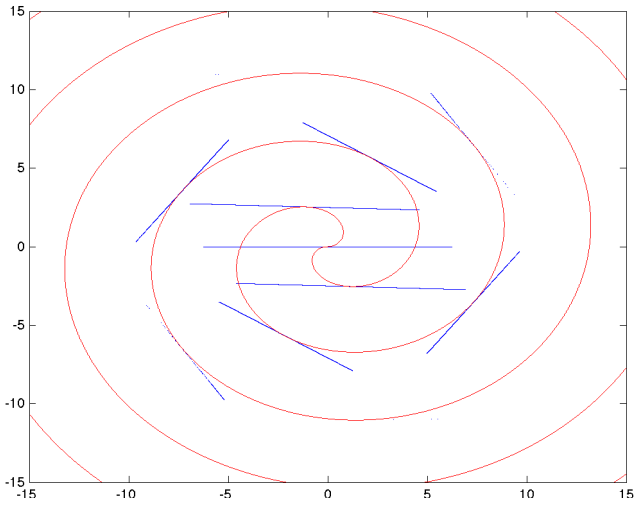

Figure 4.2: The distribution of points on the (U_1, U_2)-plane.

by applying X as inputs to a discrete memoryless channel. Now, this "side information channel" is nothing but actual channel. Namely, the first transmission serves as "side information" to the second transmission. The conception coincides with the idea of [31] except that we are discussing about Gaussian source. In detail, within power constraint P, firstly, source X is mapped to $2-$dimensional channel output U_1^* and U_2^*, where $U_1^* = \sqrt{\gamma P}X$, $U_2^* = \alpha T + \beta E$ and $\gamma P + var(U_2^*) = P$. Then transmit U_1 and U_2 (reallocated U_1^* and U_2^*) respectively through AWGN channel with noise variance σ_W^2. To make it more clear, we use figure4.4 to show the distribution of (U_1^*, U_2^*) pair. We then rotate the coordinate so that all the center points of these cluster are on x axis

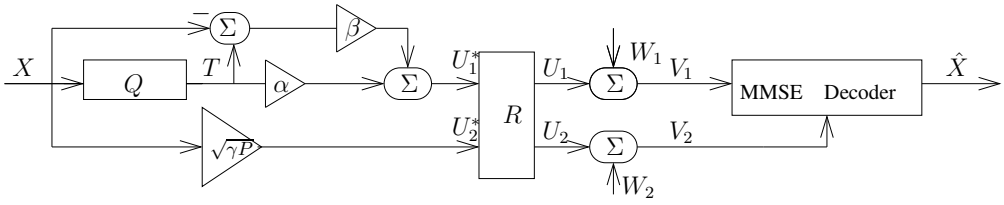

Figure 4.3: The Model of Scheme B.

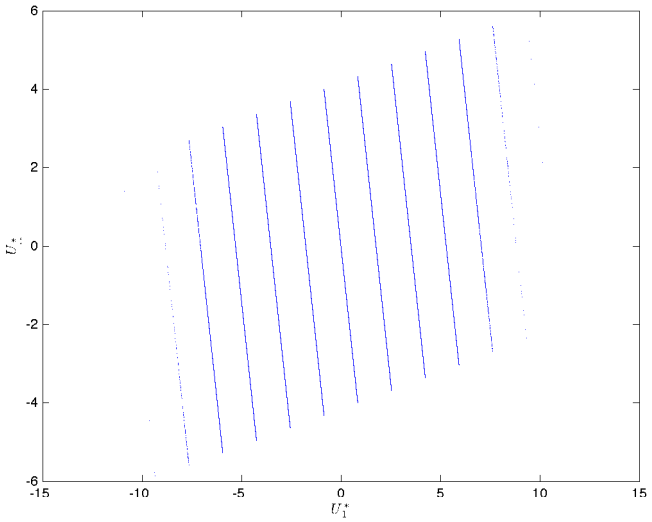

Figure 4.4: The distribution of points in the (U_1^*, U_2^*)-plane.

while power is unchanged. See figure4.5. So

$$\begin{aligned}
&\begin{bmatrix} U_1 \\ U_2 \end{bmatrix} \\
&= \frac{1}{\sqrt{\rho^2+\alpha^2}} \begin{bmatrix} \rho & \alpha \\ -\alpha & \rho \end{bmatrix} \begin{bmatrix} U_1^* \\ U_2^* \end{bmatrix} \\
&= \frac{1}{\sqrt{\rho^2+\alpha^2}} \begin{bmatrix} \rho & \alpha \\ -\alpha & \rho \end{bmatrix} \begin{bmatrix} \rho & \rho \\ \alpha & \beta \end{bmatrix} \begin{bmatrix} T \\ S \end{bmatrix}
\end{aligned}$$

Inspired by figure4.5, we could save power by reallocating the clusters as figure4.6.

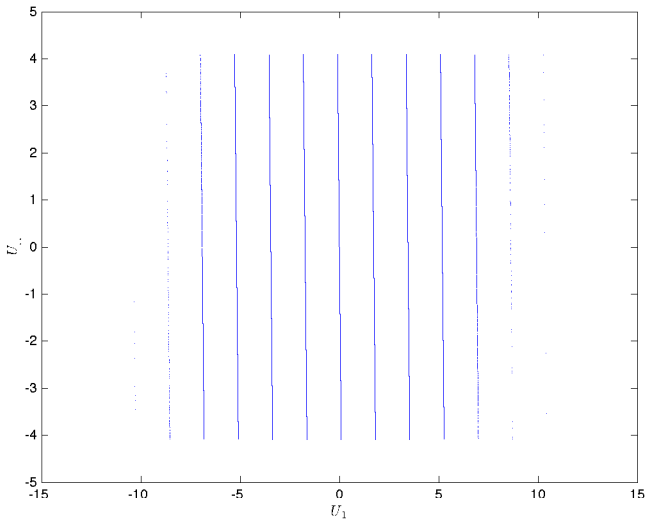

Figure 4.5: The distribution of points in the (U_1, U_2)-plane.

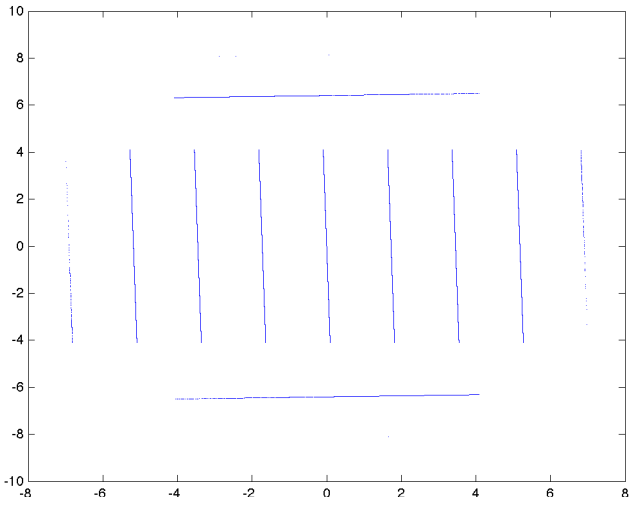

Figure 4.6: The distribution of points in the (U_1, U_2)-plane after reallocation.

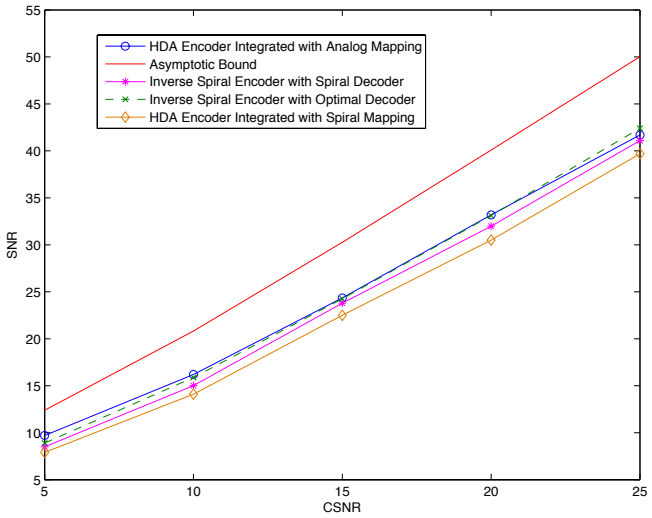

Figure 4.7: Comparison of the Channel SNR - Source SNR performance for various Schemes

4.3 Simulation Result

The simulation result is shown as 4.7. It is shown that HDA encoder combining with analog mapping performs best in low CSNR scenario while inverse spiral mapping with optimal decoder gains more advantage while CSNR becomes high. HDA encoder integrated with spiral mapping doesn't perform well as expected with highly possiblity that Δ is not small enough to make the segmentation of clusters not close enough. The space for improving exists.

Chapter 5

Conclusion and Future Work

We studied zero-delay, i.e., scalar, lossy source coding with side information at the decoder. Three related but distinct problems were investigated.

In first part, instead of imposing a periodic structure on the scalar quantizer directly, we addressed optimal quantization under the constraint that within every interval of size 2Δ, there are at most W cells. We conjectured that optimal quantizers under this regime are periodic, and proved this conjecture for the important extreme case of a very high correlation coefficient between the source and side information.

When we incorporated our zero-delay coding results into predictive coding for Gaussian sources with memory, we observed that optimal prediction in the Wyner-Ziv regime is fundamentally different from that in non-distributed coding. That is because the prediction filters must not only jointly exploit the temporal and spatial redundancies, but the prediction filter of the source must also suppress the propagation of occasional decoding errors. At low rates, the optimal action turns out to be to allow more decoding errors but prevent their propagation aggressively using a very low prediction coefficient for the source. As the rate increases, it is more advantageous to allow less decoding errors and an increased prediction coefficient.

We also employed our scalar codes in transform coding with small block lengths

(thereby achieving a low delay), where the source and side information are transformed separately. For the specific source-side information pairs studied, we showed that transform coding, even with a small block-length, outperforms predictive coding, despite the first-order Markov-like structure of the signals.

To keep our results in perspective, we also derived the asymptotic rate-distortion function for the special structure of sources we studied. Because we do not use the ideal Slepian-Wolf coding assumption anywhere in our results, the gap between the asymptotic rate-distortion function and performance of our schemes is more significant than usual.

In both the second and the third part, we studied the extreme of zero-delay hybrid digital/analog (HDA) schemes for Joint Source Channel Coding (JSCC) problem. It's investigated in two scenarios: point to point communication with side information at the decoder; 1 to 2 mapping with channel bandwidth expansion. To achieve zero-delay, after applying scalar quantization to the source, the properly scaled analog information, namely the quantization error, is superimposed on the scaled digital information, i.e., the quantized source, and then transmitted. At the decoder, several decoding schemes are proposed. Performance comparison with existing schemes is also presented. And in channel bandwidth expansion problem, we proposed two source-channel direct mapping scenarios: HDA combined with Analog Mapping and HDA Integrated with Spiral Mapping.

In [**?**], the authors proposed necessary conditions for optimality of the encoder and decoder mappings for a given finite block length. An iterative algorithm that updates encoder and decoder mappings according to these optimality conditions are proposed. We have collaborated with them by using our proposed HDA schemes as initial conditions to find the possible optimal mapping case. This is one of future work lying on.

We also would try to investigate the channel bandwidth compression scenario, for example, 2 to 1 mapping. JSCC problem with channel bandwidth mismatch when there

is side information at the decoder is also a open research area.

Bibliography

[1] B. Girod, A. Aaron, S. Rane and D. Rebollo-Monedero , "Distributed video coding," Proceedings of the IEEE, Special Issue on Video Coding and Delivery, vol. 93, no. 1, pp. 71-83, January 2005.

[2] D.Slepian and J. Wolf, "Noiseless Coding of Correlated Information Sources", *IEEE Transactions on Information Theory*, vol. 19, no. 4, pp. 471–480, July 1973.

[3] C. E. Shannon, "A mathematical theory of communication", The Bell System technical journal, 27:379423, 1948.

[4] A. D. Wyner and J. Ziv, "The rate-distortion function for source coding with side information at the decoder," *IEEE Transactions on Information Theory*, vol. 22, no. 1, pp. 1–10, January 1976.

[5] S. Zahir Azami, P. Duhamel, and O. Rioul. Joint source-channel coding: Panorama of methods. CNES Workshop on Data Compression, Toulouse, France, November 1996. http://citeseer.nj.nec.com/zahirazami96joint.html.

[6] F. Hekland. A Review of Joint Source-Channel Coding. Norwegian University of Science and Technology. http://www.iet.ntnu.no/projects/beats/Documents/JSCCreview.pdf.

[7] Y. Kochman and R. Zamir, "Joint Wyner-Ziv/Dirty-Paper Coding by Modulo-Lattice Modulation," IEEE Trans. Inform. Theory, vol. 55, no. 11, pp. 4878–4889, November 2009.

[8] M. Wilson, K. Narayanan, and G. Caire, "Joint source channel coding with side information using hybrid digital analog codes," *IEEE Trans. Inf. Theory*, vol. 56, no. 10, pp. 4922–4940, October 2010.

[9] T. J. Goblick, "Theoretical limitations on the transmission of data from analog sources," IEEE Trans. Inform. Theory, vol. 11, no. 4, pp. 558–567, October 1965.

[10] S. Shamai, S. Verdu, and R. Zamir, "Systematic lossy source/channel coding," *IEEE Trans. Inf. Theory*, vol. 44, no. 2, pp. 564–579, March 1998.

[11] R. Zamir and S. Shamai, "Nested linear/lattice codes for Wyner-Ziv encoding," *Proc. IEEE Information Theory Workshop*, pp. 92-93, Killarney, Ireland, June 1998.

[12] R. Zamir, S. Shamai, and U. Erez, "Nested linear/lattice codes for structured multiterminal binning," *IEEE Transactions on Information Theory*, vol. 48, no 6, pp. 1250-1276, June 2002.

[13] S. Pradhan and K. Ramchandran, "Distributed source coding using syndromes (DISCUS): Design and construction," *IEEE Transactions on Information Theory*, vol. 49, no. 3, pp. 626-643, March 2003.

[14] Z. Liu, S. Cheng, A. D. Liveris and Z. Xiong, "Slepian-Wolf coded nested lattice quantization for Wyner-Ziv coding: High-rate performance analysis and code design," *IEEE Transactions on Information Theory*, vol. 52, no. 10, pp. 4358-4379, October 2006.

[15] A. Liveris, Z. Xiong, and C. Georghiades, "Compression of binary sources with side information at the decoder using LDPC codes," *IEEE Communications Letters*, vol. 6, pp. 440-442, October 2002.

[16] Z. Xiong, A. Liveris, S. Cheng, and Z. Liu, "Nested quantization and Slepian-Wolf coding: A Wyner-Ziv coding paradigm for i.i.d. sources," *Proc. IEEE Workshop on Statistical Signal Processing*, St. Louis, MO, September 2003.

[17] Y. Yang, S. Cheng, Z. Xiong, and W. Zhao, "Wyner-Ziv coding based on TCQ and LDPC codes" *IEEE Transactions on Communications*, vol. 57, pp. 376–387, February 2009.

[18] J. Kusuma, L. Doherty and K. Ramchandran, "Distributed compression for sensor networks," *Proc. IEEE International Conference on Image Processing*, Thessaloniki, Greece, 2001.

[19] S. D. Servetto, "Lattice quantization with side information: Codes, asymptotics, and applications in sensor networks," *IEEE Transaction on Information Theory*, vol. 53, no. 2, pp. 714-731, February 2007.

[20] R. Zamir, "Lattices are everywhere," *Information Theory and Applications*, San Diego, February 2009.

[21] A. Saxena and K.Rose, "Distributed predictive coding for spatio-temporally correlated sources," *IEEE Transactions on Signal Processing*, vol. 57, no. 10, October 2009.

[22] E. Tuncel, "Predictive coding of correlated sources," *Proc. IEEE Information Theory Workshop*, pp. 111–116, San Antonio, TX, October 2004.

[23] J. Nayak and E. Tuncel, "Low-delay quantization for source coding with side information," *IEEE International Symposium on Information Theory*, Toronto, CA, July 2008.

[24] M. Gastpar, P. L. Dragotti, and M. Vetterli, "The distributed Karhunen-Loève transform." *IEEE Transactions on Information Theory*, vol. 52, no. 12, pp. 5177-5196, December 2006.

[25] D. Rebollo-Monedero and B. Girod, "Quantization for distributed source coding," *In Distributed Source Coding: Theory, Algorithm and Applications*, eds. P. L. Dragotti and M. Gastpar, Academic Press, Elsevier, San Diego, CA, 2009.

[26] D. Rebollo-Monedero, S. Rane, A. Aaron, and B. Girod. "High-rate quantization and transform coding with side information at the decoder." *EURASIP Signal Processing Journal*, vol. 86, no. 11, pp. 3160–3179, November 2006. Special Issue on Distributed Source Coding.

[27] S. S. Pradhan and K. Ramchandran, "Distributed compression in a dense microsensor network," *IEEE Signal Processing Magazine*, vol. 19, no. 2, pp. 51–60, March 2002.

[28] T. Berger, *Rate Distortion Theory. A Mathematical Basis for Data Compression*, Prentice-Hall, Englewood Cliffs, NJ, 1971.

[29] A. Gersho and R. Gray, *Vector Quantization and Signal Compression*, Kluwer Academic Press, 1992.

[30] R. Gray, "Toeplitz and circulant matrices: A review," *Foundations and Trends in Communications and Information Theory*, Now Publishers, vol. 2, no. 3, 2006.

[31] B.Chen and G. W. Wornell, "Analog Error-Correcting Codes Based on Chaotic Dynamical Systems," IEEE Trans. Communications, vol. 46, no. 7, pp.881-890, July 1998

[32] I.Kvecher and D.Rephaeli, "An Analog Modulation Using a Spiral Mapping," IEEE 24th Convention of Electrical and Electronics Engineers in Israel, 2006

[33] F. Hekland, G E.Oien and T. A. Ramstad, "Using 2:1 Shannon Mapping fror Joint Source-Cannel Coding," Data Compression Conference, 2005.

[34] E. Akyol, K. Rose, "Towards Optimality of Analog Mappings for Source Channel Coding," IEEE Transactions on Communications, under review.

Appendix A

The Asymptotic Rate-Distortion Tradeoff

Theorem 16 *The Wyner-Ziv rate-distortion function for the pair $(X(n), Y(n))$ described in (2.28) and (2.29) for any stationary Gaussian $T(n)$ is parameterized as*

$$R_\theta = \frac{1}{4\pi} \int_{-\pi}^{\pi} \max \left[0, \log \frac{A(e^{j\omega})}{\theta} \right] d\omega \tag{A.1}$$

and

$$D_\theta = \frac{1}{2\pi} \int_{-\pi}^{\pi} \min \left[\theta, A(e^{j\omega}) \right] d\omega \tag{A.2}$$

where

$$A(e^{j\omega}) = \Phi_{XX}(e^{j\omega}) - \frac{\Phi_{XY}(e^{j\omega})^2}{\Phi_{YY}(e^{j\omega})}$$

and where $\Phi_{XX}(e^{j\omega})$, $\Phi_{YY}(e^{j\omega})$, and $\Phi_{XY}(e^{j\omega})$ are the discrete-time Fourier transforms (DTFT) of $R_{XX}(\tau)$, $R_{YY}(\tau)$, and $R_{XY}(\tau)$, respectively.

Proof. For the given source model, following the same logic as in Section 2.5, we can deduce that by applying the same de-correlating transformation $\mathbf{A}$ to both sources, i.e., obtain $\mathbf{X'} = \mathbf{AX}$ and $\mathbf{Y'} = \mathbf{AY}$ with $\mathbf{X} = [X(1)\ X(2)\ \ldots\ X(n)]^T$ and $\mathbf{Y} = [Y(1)\ Y(2)\ \ldots\ Y(n)]^T$, all three covariance matrices $\mathbf{C_{XX}}$, $\mathbf{C_{YY}}$, and $\mathbf{C_{XY}}$ are diagonalized simultaneously. This, in turn, implies that transform coefficient pairs (X'_k, Y'_k)

are independent of each other and thus can be coded separately with optimal rate

$$R_\theta(k) = \max\left[0, \frac{1}{2}\log\frac{\sigma^2_{X'_k}(1-\rho^2_{X'_kY'_k})}{\theta}\right] \tag{A.3}$$

and distortion

$$D_\theta(k) = \min\left[\theta, \sigma^2_{X'_k}(1-\rho^2_{X'_kY'_k})\right] \tag{A.4}$$

for some $\theta > 0$, where the formulas (A.3) and (A.4) follow by generalizing the optimal (i.e., water-filling) bit allocation discussed in [28] to Wyner-Ziv rate-distortion function [4]. The relevant quantity $\sigma^2_{X'_k}(1-\rho^2_{X'_kY'_k})$ can be expressed as

$$\begin{aligned}\sigma^2_{X'_k}(1-\rho^2_{X'_kY'_k}) &= \lambda^k_{\mathbf{XX}}\left(1-\frac{(\lambda^k_{\mathbf{XY}})^2}{\lambda^k_{\mathbf{XX}}\lambda^k_{\mathbf{YY}}}\right)\\ &= \lambda^k_{\mathbf{XX}}-\frac{(\lambda^k_{\mathbf{XY}})^2}{\lambda^k_{\mathbf{YY}}}\\ &\triangleq \lambda^k\end{aligned} \tag{A.5}$$

where $\lambda^k_{\mathbf{XX}}$, $\lambda^k_{\mathbf{YY}}$, and $\lambda^k_{\mathbf{XY}}$ are the kth *eigenvalues* of $\mathbf{C_{XX}}$, $\mathbf{C_{YY}}$, and $\mathbf{C_{XY}}$, respectively. We observe that λ^k is the kth eigenvalue of

$$\mathbf{C} \triangleq \mathbf{C_{XX}} - \mathbf{C_{XY}}^2\mathbf{C_{YY}}^{-1}\,.$$

This follows because $\mathbf{A}$ also diagonalizes $\mathbf{C}$.

Now, [30, Theorem 4.2] shows that for an infinite Toeplitz matrix $\mathbf{T}$ with entries t_k on the top row, and for any function F that is continuous on the range of the eigenvalues $\lambda^k_{\mathbf{T}}$ of $\mathbf{T}$,

$$\lim_{n\to\infty}\frac{1}{n}\sum_{k=1}^{n}F\left(\lambda^k_{\mathbf{T}}\right) = \frac{1}{2\pi}\int_{-\pi}^{\pi}F\left[\Phi(\omega)\right]d\omega$$

where $\Phi(\omega)$ is the DTFT of t_k. Further, [30, Theorem 5.2(c)] and [30, Theorem 5.3(b)] state that

$$\lim_{n\to\infty}\frac{1}{n}\sum_{k=1}^{n}F\left(\lambda^k_{\mathbf{T}^{-1}}\right) = \frac{1}{2\pi}\int_{-\pi}^{\pi}F\left[\frac{1}{\Phi(\omega)}\right]d\omega$$

and

$$\lim_{n\to\infty}\frac{1}{n}\sum_{k=1}^{n}F\left(\lambda^k_{\mathbf{T}_1\mathbf{T}_2}\right) = \frac{1}{2\pi}\int_{-\pi}^{\pi}F\left[\Phi_1(\omega)\Phi_2(\omega)\right]d\omega$$

respectively, where $\Phi_i(\omega)$, $i = 1, 2$, are the DTFT of the top row of $\mathbf{T}_i$. Choosing $F(\lambda^k) = \max\left[0, \frac{1}{2}\log\frac{\lambda^k}{\theta}\right]$ and $F(\lambda^k) = \min\left[\theta, \lambda^k\right]$ as in (A.3) and (A.4) respectively yield (A.1) and (A.2). ■